Zeniya T, Hirano Y, Sakimoto T, Ishida K, WatabeH, Teramoto N, Kudo H, Minato K, Hatazawa J, Iida H	Conceptual design of high resolution and quantitative SPECT system for imaging a selected small ROI of human brain	*2009 IEEE Nuclear Science Symposium ConferenceRecord*	174
Huang Q, Zeniya T, KudoH, Iida H, Gullbereg G	Interior SPECT reconstruction problem with tiny a priori knowledge - An application for high resolution pinhole brain imaging	*Proceedings of 10th International Meeting on Fully Three-Dimensional Image Reconstruction in Radiology and Nuclear Medicine*	177
de Jong HW, Lubberink M, Watabe H, Iida H, Lammertsma AA	A method to measure PET scatter fractions for daily quality control	*Med Phys*	181

Applied Radiation and Isotopes ▮ (▮▮▮▮) ▮▮▮–▮▮▮

Contents lists available at ScienceDirect

Applied Radiation and Isotopes

journal homepage: www.elsevier.com/locate/apradiso

Electrochemical concentration of no-carrier-added [^{18}F]fluoride from [^{18}O]water in a disposable microfluidic cell for radiosynthesis of ^{18}F-labeled radiopharmaceuticals

Hidekazu Saiki [a], Ren Iwata [b,*], Hiroaki Nakanishi [a], Rebecca Wong [b], Yoichi Ishikawa [b], Shozo Furumoto [b], Ryo Yamahara [a], Katsumasa Sakamoto [a], Eiichi Ozeki [a]

[a] Technology Research Laboratory, Shimadzu Corporation, Kyoto 619-0237, Japan
[b] Cyclotron and Radioisotope Center, Tohoku University, Sendai 980-8578, Japan

ARTICLE INFO

Article history:
Received 27 October 2009
Received in revised form
26 January 2010
Accepted 6 February 2010

Keywords:
Microfluidics
Electrochemical concentration
Automation
Fluorine-18 fluoride

ABSTRACT

The realization of the electrochemical method for microfluidic radiosynthesis is described for concentrating aqueous no-carrier-added [^{18}F]fluoride into an aprotic solvent in a disposable microfluidic cell. Flowing aqueous [^{18}F]fluoride was introduced into a disposable microfluidic cell (16 μL) under an electric potential (10 V), followed by anhydrous MeCN. The trapped [^{18}F]fluoride was released in MeCN containing Kryptofix® 222–$KHCO_3$ (ca. 60 μL) under heat and a reversed potential (−2.5 V). An automated module provided the [^{18}F]fluoride ready for subsequent microfluidic radiosynthesis in overall radiochemical yields of 60% within 6 min.

1. Introduction

Positron emission tomography (PET) is recognized as a powerful tool for in vivo molecular imaging and its use in the discovery and early development of drug candidates has been increasing. The four commonly used PET radionuclides (^{11}C, ^{13}N, ^{15}O and ^{18}F) are relatively short-lived, which creates many obstacles towards extensive applications. However, ^{18}F has a longer half-life (109.8 min) than the others and is more attractive for synthetic and clinical use. ^{18}F-labeled radiopharmaceuticals were initially produced in the 1970s with the radiosynthesis of 2-deoxy-2-[^{18}F]fluoro-D-glucose ([^{18}F]FDG) from [^{18}F]F_2 (Ido et al., 1978). The first successful application of the Kryptofix® 222 (K.222)-assisted substitution of no-carrier-added (n.c.a.) [^{18}F]fluoride to [^{18}F]FDG synthesis (Hamacher et al., 1986) accelerated further development and evaluation of new ^{18}F-labeled compounds.

The ^{18}O(p,n)^{18}F reaction on enriched [^{18}O]water is the current preferred method. It has high production yield and specific activity (theoretical specific activity: 6.33×10^{10} GBq/mol). While it is decreased to a considerable extent in the production and radiosynthesis processes, the specific activity of n.c.a ^{18}F-labeled products is sufficiently high, and the synthesis utilizing [^{18}F]fluoride can in principle be classified as a microscale reaction.

[^{18}F]Fluoride is usually separated from 1 to 2 mL of the target [^{18}O]water by anion exchange (Schlyer et al., 1990), often with a Sep-Pak Light Accell QMA cartridge (Waters). The [^{18}F]fluoride is then eluted with potassium carbonate dissolved in a small quantity of water or an acetonitrile–water mixture. Repeated azeotropic evaporation of water–acetonitrile is required to remove the water that accompanies this procedure from the aqueous [^{18}F]fluoride, and subsequent nucleophilic substitution in an aprotic solvent is then possible. A few proof-of-concept studies of microfluidic radiosynthesis of ^{18}F-radiopharmaceutical have been reported. Each of these has utilized the [^{18}F]KF–K.222 complex ([K^+/K.222]$^{18}F^-$) in an anhydrous solvent prepared by this conventional drying method (Liow et al., 2005; Gillies et al., 2006a, b; Wester et al., 2009) but not directly from aqueous [^{18}F]fluoride. One method reportedly used about 1 μL of the target water with their microfluidic device (Lee et al., 2005). Those approaches are common because to date no practical interfacing method has been developed for rapidly introducing 1–2 mL of the target water into a microfluidic device and efficiently converting aqueous [^{18}F]fluoride to the reactive [^{18}F]fluoride.

An electrochemical procedure was thought to be a potential method to rapidly concentrate aqueous [^{18}F]fluoride into an organic solvent. It was first developed for [^{18}F]fluoride recovery from [^{18}O]water (Alexoff et al., 1989). [^{18}F]Fluoride was electrically

* Corresponding author. Tel./fax: +81 22 795 7798.
E-mail address: rencyric@cyric.tohoku.ac.jp (R. Iwata).

0969-8043/$ - see front matter © 2010 Published by Elsevier Ltd.
doi:10.1016/j.apradiso.2010.02.005

Please cite this article as: Saiki, H., et al., Electrochemical concentration of no-carrier-added [^{18}F]fluoride from [^{18}O]water in a disposable microfluidic cell for radiosynthesis of ^{18}F-labeled radiopharmaceuticals. Appl. Radiat. Isotopes (2010), doi:10.1016/j.apradiso.2010.02.005

deposited onto a carbon anode in a cell and then released into normal water by applying reversed voltages. The method was further improved by efficiently recovering the deposited [^{18}F]fluoride in an aprotic solvent containing the dissolved potassium–K.222 complex and proceeding with ^{18}F-fluorination in the same cell (Hamacher and Blessing, 1995; Hamacher et al., 2002; Reischl et al., 2002; Hamacher and Coenen, 2006). In the present study, we describe an innovative conversion of the above static method to a flow method for convenient and efficient concentration of n.c.a. [^{18}F]fluoride in a disposable microfluidic cell that can provide a practical interface with microfluidic radiosynthesis of ^{18}F-labeled radiopharmaceuticals. While preparing the manuscript, a similar development was presented at the 18th International Symposium on Radiopharmaceutical Sciences, July 12–17, 2009, Edmonton (Rensch et al., 2009) and an outline of the present study was also presented at the symposium (Saiki et al., 2009).

2. Materials and methods

[^{18}O]Water (> 97 atom%-enrichment) was purchased from Taiyo Nippon Sanso and used as a target for the ^{18}O(p,n)^{18}F reaction. K.222 was obtained from Merck, potassium bicarbonate ($KHCO_3$), and anhydrous acetonitrile (MeCN) from Sigma-Aldrich, and 1,3,4,6-tetra-*O*-acetyl-2-*O*-trifluoro-methanesulfonyl-*β*-D-mannopyranose (mannose triflate) from ABX and Wako Pure Chemicals.

An appropriate amount of K.222 was dissolved in anhydrous MeCN and then $KHCO_3$ was added (molar ratio K.222/$KHCO_3$=1.1) and stirred until it was completely dissolved. The solvent was evaporated to dryness under reduced pressure to give the residual K.222–$KHCO_3$ complex. An approximately 40 mM equivalent solution of the complex in anhydrous MeCN was prepared and used for the experiment.

HPLC analysis was performed on an ODS column (YMC-Pack Pro C18RS, 150 × 4.6 mm, YMC) with an HPLC system (Shimadzu Prominence LC-20AD and SPD-20A) connected to a radiation detector (US3000, Universal Engineering Corp., Japan). The selected solvent was a mixture of acetonitrile and water (40:60, v/v).

2.1. Electrochemical microfluidic cell and peripheral devices

The disposable electrochemical microfluidic cell consisted of two adhered plates of quartz and PDMS (poly(dimethylsiloxane)) resin (60 × 15 × 4 mm) (Fig. 1). The inner flow channel was 100 μm high, 4 mm wide and 40 mm long with a volume of 16 μL. The quartz plate was sputtered with Pt on the inner surface and had inlet and outlet ports. The PDMS resin plate had a glassy carbon (GC) electrode on the inner surface and two holes on the back that allowed Pt and carbon electrodes to contact with probes

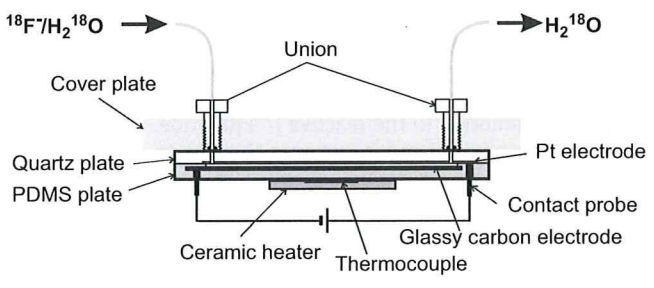

Fig. 1. Side view of an electrochemical microfluidic cell.

through which the electric field was supplied (Regulated DC Power Supply PW18-1.8Q, Kenwood). The cell was typically placed facing upwards on an Al plate (40 × 20 × 4 mm^3) connected to a 100 W micro-ceramic heater (MS-1, Sakaguchi E.H VOC Corp.). The temperature was monitored with a thermocouple sheet (Sakaguchi E.H VOC Corp.). Liquid flow was controlled using an infusion pump (KDS 210 Syringe Pump, KD Scientific).

2.2. Deposition and release of [^{18}F] fluoride

[^{18}F]Fluoride was produced with a Cypris HM-12 cyclotron (Sumitomo Heavy Industries) at the Cyclotron and Radioisotope Center of Tohoku University. Typically, a 700 μL aliquot of [^{18}O]water in a Ti-chamber was irradiated with a 12-MeV proton beam current of 30 μA for 40–60 min. It was then recovered into a glass vial through PEEK tubing and diluted, if necessary, with natural water for subsequent experiments.

A 1.5 mL aliquot of water containing [^{18}F]fluoride (100–500 MBq) was passed through the cell at a flow rate of 0.1–1.0 mL/min under a constant electric potential (1–10 V) applied between the Pt cathode and GC anode. The cell was then flushed with anhydrous MeCN (1.0 mL/min, 2 min) under the same electric potential and the voltage was disconnected.

Two methods, flow and stop-flow, were investigated to optimize the release of deposited [^{18}F]fluoride into the MeCN solution containing K.222–$KHCO_3$. In the flow method, the K.222–$KHCO_3$ was allowed to flow continuously (200 μL/min) under a reversed potential (approximately −3 to −1 V) while the cell was heated to a preset temperature (80–100 °C). Flow was maintained until all the released [^{18}F]fluoride was collected into a vial. Since the release of [^{18}F]fluoride was not a prompt process, the following stop-flow method was expected to afford a much less volume of the recovered [^{18}F]fluoride solution than the flow method. The cell was first filled with the K.222–$KHCO_3$ solution and flow was then temporarily halted. The cell was then immediately heated to a preset temperature and a reversed potential was applied simultaneously. This continued for a preset time (0.5–3 min) before flow was allowed to resume to a rate of 200 μL/min. The released [^{18}F]fluoride was then collected into a vial. In both methods, the [K^+/K.222]$^{18}F^-$ solution was flowed through a Tefzel tube (inner diameter 0.25 mm) and monitored with an NaI(Tl) scintillation detector (Flow-Count with a FC-3100 PMT/Scintillation detector, Bioscan) to estimate its net volume from the elution profiles.

Distribution images of [^{18}F]fluoride on a GC plate were obtained with an imaging plate system (Fuji Bio-Imaging Analyzer BAS 5000).

2.3. Automated module

An automated module was developed for routine preparation of the [K^+/K.222]$^{18}F^-$ solution with the optimized procedure (Fig. 2). Four syringe pumps (SP 1–4, PSD/3 Syringe pump module, Hamilton) equipped with a T-valve and a 0.5 or 2.5 mL syringe were used to transfer liquids. Four-port distribution and 6-way valves (IV and OV, Modular Valve Positioners, Hamilton) were used to regulate liquid transfer. A disposable flow-cell chip was fixed to a platform through which heat and electrical potential were supplied. The entire module was controlled through dedicated PC software. Five optimized concentration procedures were sequentially executed (Table 1). The sequence was initiated by filling each syringe with its respective liquid immediately after collecting aqueous [^{18}F]fluoride into the starting vial. The released [K^+/K.222]$^{18}F^-$ solution was transferred into a loop (100 μL) connected to the outlet 6-way valve (OV). It was then

Please cite this article as: Saiki, H., et al., Electrochemical concentration of no-carrier-added [^{18}F]fluoride from [^{18}O]water in a disposable microfluidic cell for radiosynthesis of ^{18}F-labeled radiopharmaceuticals. Appl. Radiat. Isotopes (2010), doi:10.1016/j.apradiso.2010.02.005

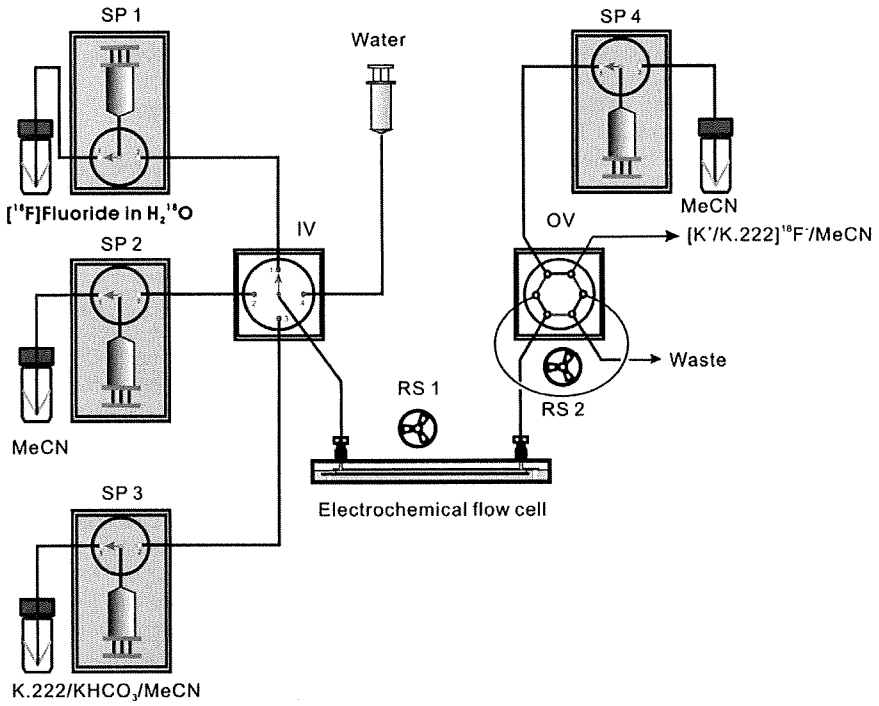

Fig. 2. Schematic diagram of the automated module; SP 1-4, PSD/3 syringe pump; IV, 4-port distribution valve; OV, 6-way valve; RS 1-2, radiation sensor.

Table 1
Sequence of the automated procedure.

Sequence no.	Procedure	Aqueous [^{18}F]fluoride		MeCN		[K/K.222]HCO_3/MeCN		Potential (V)	Temp.	Processing time (min)
		Volume	Flow rate	Volume	Flow rate	Volume	Flow rate			
1	Charge-up	2.0 mL[a]	max.	2.5 mL	max.	500 μL	max	0	r. t.	0.2
2	Deposition	2.0 mL	700 μL/min	–	–	–	–	+10.0	r. t.	2.8
3	Washing	–	–	2.0 mL	5.0 mL/min	–	–	+10.0	r. t.	0.4
4	Release	–	–	–	–	125 μL	200 μL/min	0	r. t.	0.63
		–	–	–	–	–	–	−2.5	80 °C	1.0
5	Recovery/transfer	–	–	–	–	150 μL	200 μL/min	−2.0	80 °C	0.75
										(Total running time: 5.78 min)

[a] 1.5 mL [^{18}F]fluoride water solution plus 0.5 mL air that was used to push out the remaining water from the cell.

sent to a microfluidic chip with a syringe pump (SP 4). For each repeated use, the flow cell was washed with water (2 mL). ^{18}F-radioactivities were monitored with two radiation sensors (RS 1 and 2, UG-SPD-03, Universal Engineering Corp., Japan) at the flow cell and the loop.

2.4. Radiosynthesis of [^{18}F]FDG

Radiosynthesis of [^{18}F]FDG was carried out to evaluate the reactivity of the recovered $[K^+/K.222]^{18}F^-$ in MeCN. The $[K^+/K.222]^{18}F^-$ solution (ca. 0.2 mL) was added to a vial containing mannose triflate (20 mg) dissolved in anhydrous MeCN (1 mL) and heated at 80oC for 5 min. The reaction was quenched by adding water (5 mL) and the resulting solution was passed through an activated Sep-Pak tC18 cartridge followed by washing with water (5 mL). The ^{18}F radioactivity retained by the cartridge was assigned to the protected [^{18}F]FDG.

The ^{18}F-substitution of mannose triflate using $[K^+/K.222]^{18}F^-$ in MeCN with a microfluidic reactor was also demonstrated. As described above the MeCN solution of $[K^+/K.222]^{18}F^-$ in the loop was injected into a quartz flow-cell (200 μm width × 150 μm depth; cell volume, 100 μL) heated at 80 °C using the Syringe pump 4 (SP 4) after switching the 6-way valve (OV) and made to mix at the inlet with the mannose triflate in MeCN (20 mg/mL) solution flowed with additional syringe pump, both at the same flow rate. The combined solution was flowed through the cell and collected into a vial containing a small quantity of water for quenching the reaction. Reaction time was varied by adjusting the flow rate. The ^{18}F-substitution yields were determined by HPLC analysis.

3. Results and discussion

3.1. Deposition of [^{18}F]fluoride

In the preceding two studies [^{18}F]fluoride was statically deposited onto a carbon electrode in an electrochemical cell, and the volume of solvent for recovery of [^{18}F]fluoride from the electrode was then in principle the same as that of the irradiated

Please cite this article as: Saiki, H., et al., Electrochemical concentration of no-carrier-added [^{18}F]fluoride from [^{18}O]water in a disposable microfluidic cell for radiosynthesis of ^{18}F-labeled radiopharmaceuticals. Appl. Radiat. Isotopes (2010), doi:10.1016/j.apradiso.2010.02.005

target water (typically 1–2 mL) (Alexoff et al., 1989; Hamacher et al., 2002). A reduction in this solvent volume translates to less cell volume required in the development of an electrochemical flow cell for trapping [^{18}F]fluoride from flowing water. Obviously, the efficiency of trapping [^{18}F]fluoride depends, at least among several expected parameters, on the electric field strength between the cathode and anode and the dwell time of [^{18}F]fluoride in the cell. The electric potential and the distance between the electrodes determine the former and the correlation between the flow rate of the water and the cell volume the latter. Consequently, the electrode distance is a more crucial dimension than others. The flow cell was designed with a 100 μm height and a 4 × 40 mm electrode surface area. This short distance allowed [^{18}F]fluoride to rapidly move to the GC surface from the flowing water as well as produced higher electric field strength (V/cm) with lower potential. The [^{18}F]fluoride deposition was rapidly increased up to 80% at 3 V followed by a gradual increase over 90% at 10 V (Fig. 3). These high efficiencies were achievable due to a short dwell time in the flow cell (16 μL), estimated to be ca. 5 s at the flow rate of 200 μL/min and high field strength in the present system. The amount of [^{18}F]fluoride deposited in response to dwell time (i.e., flow rate) with different potentials is shown in Fig. 4. No significant decrease in the efficiency was seen with increased flow rate at 10 V. A higher flow rate is generally more advantageous for the short-lived ^{18}F; therefore, 10 V and 700 μL/min were chosen as the optimal parameters for the automated deposition procedure.

3.2. Recovery of [^{18}F]fluoride

Effects of reversed electric potential, temperature and time required for releasing [^{18}F]fluoride from the GC surface were investigated. A decrease in released [^{18}F]fluoride yield was obtained by lowering the potential below −1.5 V (Fig. 5) and a voltage of −2 V was chosen for efficient release of [^{18}F]fluoride. With this optimal voltage [^{18}F]fluoride was very rapidly released from the GC surface and reached a maximum release almost within 1 min, with no further increase afterwards (Fig. 6). Heating was observed to remarkably enhance the release of [^{18}F]fluoride. These observations are consistent with a previous report (Hamacher et al., 2002). Thus, automated [^{18}F]fluoride release was carried out using the stop-flow method at 80 °C and −2 V for 1 min.

For radiosynthesis use of the recovered [^{18}F]fluoride in a microfluidic reactor, the volume is crucial and a minimal volume is desirable. The volume in this case was estimated to be approximately 60 μL from the [^{18}F]fluoride elution profile. This was relatively high compared with the 16 μL volume of the flow cell, and may be ascribed to diffusion while transferring the [^{18}F]fluoride solution from the flow-cell to the loop especially in the outlet valves where dead space between fittings was

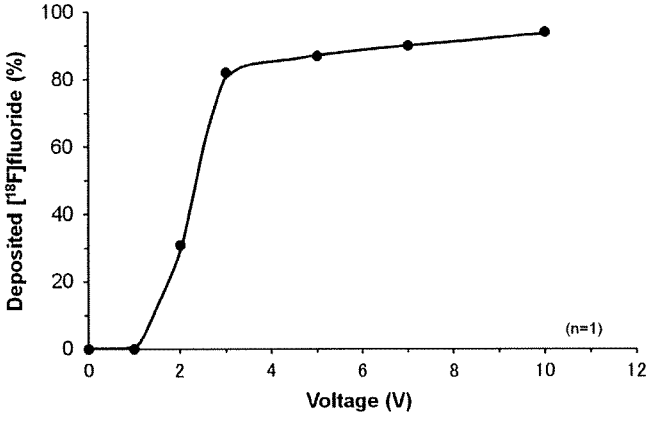

Fig. 3. Dependence of [^{18}F]fluoride deposition on electric potential, with a flow rate of 200 μL/min.

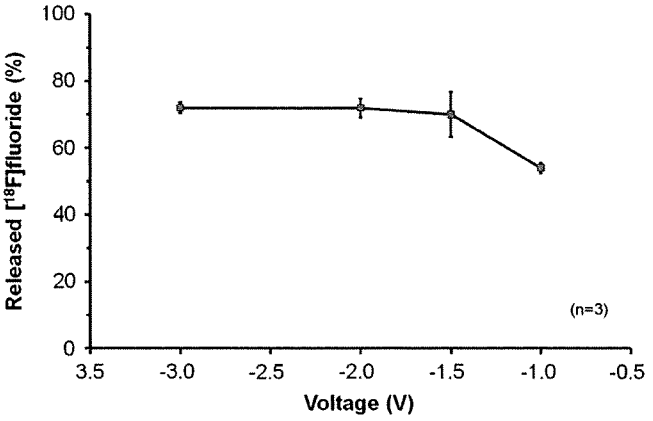

Fig. 5. Voltage dependence of [^{18}F]fluoride release into the [K/K.222]HCO_3–MeCN solution at 80 °C (stop-flow method).

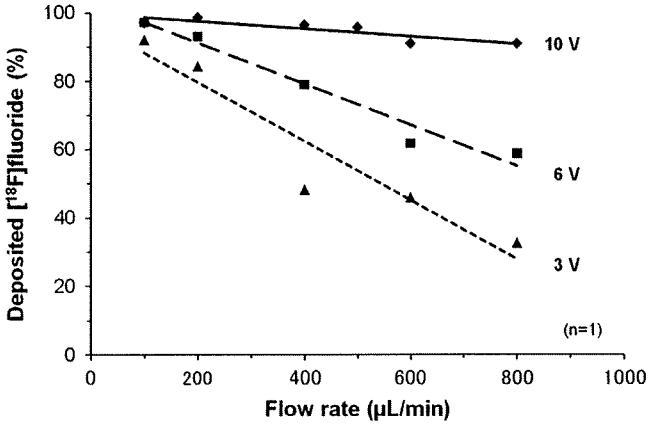

Fig. 4. Correlation between [^{18}F]fluoride deposition and a flow rate dependent on electric potential.

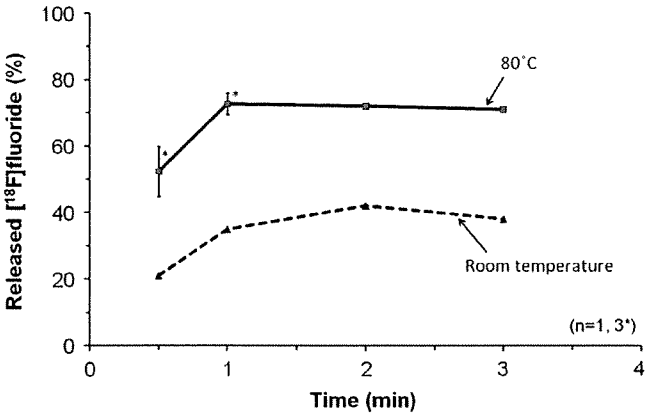

Fig. 6. Time dependence of [^{18}F]fluoride release into the [K/K.222]HCO_3–MeCN solution at −2 V (stop-flow method).

Please cite this article as: Saiki, H., et al., Electrochemical concentration of no-carrier-added [^{18}F]fluoride from [^{18}O]water in a disposable microfluidic cell for radiosynthesis of ^{18}F-labeled radiopharmaceuticals. Appl. Radiat. Isotopes (2010), doi:10.1016/j.apradiso.2010.02.005

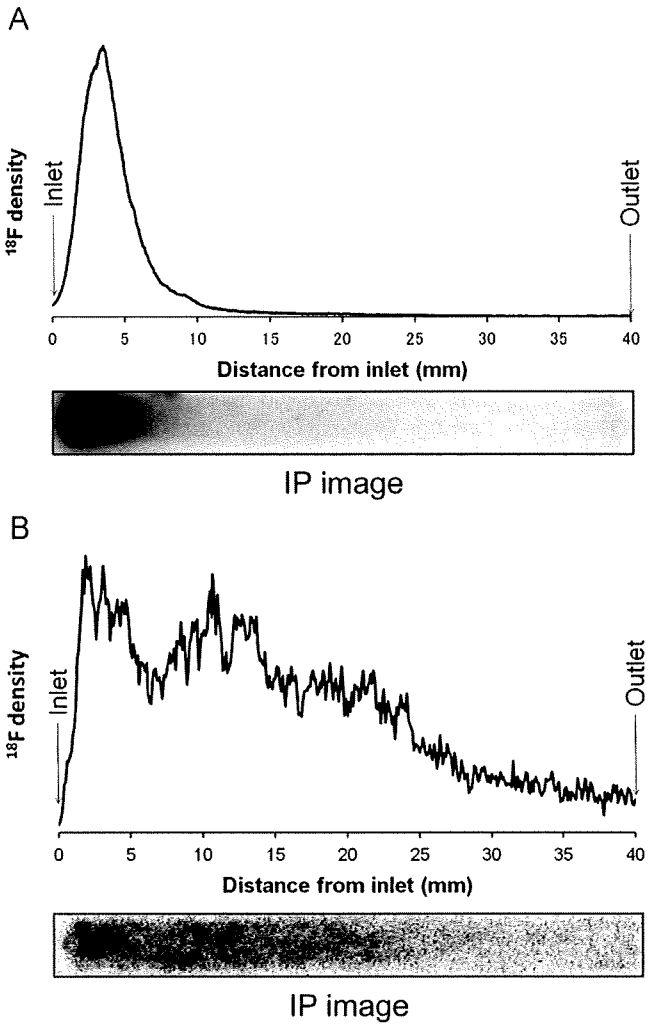

Fig. 7. IP image (lower) and distribution profile (upper) of ^{18}F on a glassy carbon plate: (A) flow rate, 200 μL/min and (B) flow rate, 700 μL/min.

not negligible. Nevertheless, the concentration of [^{18}F]fluoride solution ready for microfluidic reactions was achieved for the first time using the present flow cell although a similar thin planar cell design was suggested in the patent (Hamacher and Blessing, 1995).

The distribution of [^{18}F]fluoride on the GC plate helps optimize the size of the flow cell. As clearly seen in the image profiles of the deposited ^{18}F (Fig. 7), most of [^{18}F]fluoride was trapped in the first quarter of the GC surface area at a flow rate of 200 μL/min, while at a flow rate of 700 μL/min it was deposited over the whole area of the plate. These results suggest the possibility of reducing the flow path to 1/4 of that of the present cell without decreasing the deposition efficiency at 200 μL/min; although the target water would take three-times as long to flow, leading to a decrease in the volume of the recovered [K^+/K.222]$^{18}F^-$ solution.

3.3. *Automated procedure for concentration of [^{18}F]fluoride*

Automation in preparation of PET radiopharmaceuticals is not only convenient for performing routines consisting of several sequences but also useful for minimizing the operation time. The stop-flow method was adopted for the automated electrochemical concentration module. The total processing time needed from deposition to release of [^{18}F]fluoride was less than 6 min (Table 1). Liquid transfer could be preciously and reproducibly controlled using syringe pump modules and switching valves. One of the advantages of the microfluidic cell is that the short distance between the electrodes provides high electric field strength under such low electric potentials, which can be easily made available from commercial DA converter chips. Thus, the automated module did not require dedicated apparatus such as a switching regulator.

From typical ^{18}F-radioactivity profiles monitored at the flow cell and the transfer loop (Fig. 8), it can be clearly seen that ^{18}F linearly accumulated on the cell during the deposition process and it was not decreased by washing with MeCN. ^{18}F-radioactivity was promptly transferred into the loop and gradual decrease in the loop showed a slow transfer of a 60–80 μL of [K/K.222]^{18}F solution to a microfluidic reaction cell at a flow rate of 20 μL/min. The profile also clearly indicates that nearly 40% of the trapped

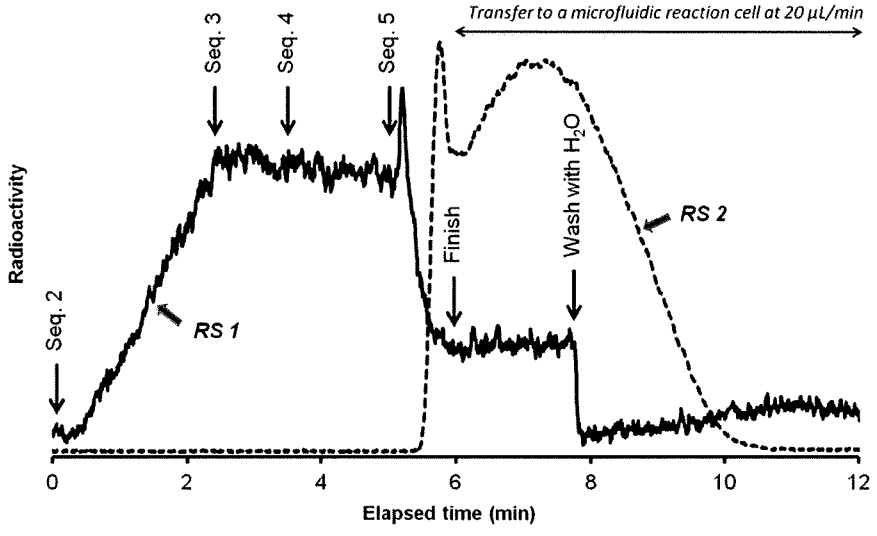

Fig. 8. Monitoring of ^{18}F-radioactivities at the concentration flow cell and the transfer loop.

Please cite this article as: Saiki, H., et al., Electrochemical concentration of no-carrier-added [^{18}F]fluoride from [^{18}O]water in a disposable microfluidic cell for radiosynthesis of ^{18}F-labeled radiopharmaceuticals. Appl. Radiat. Isotopes (2010), doi:10.1016/j.apradiso.2010.02.005

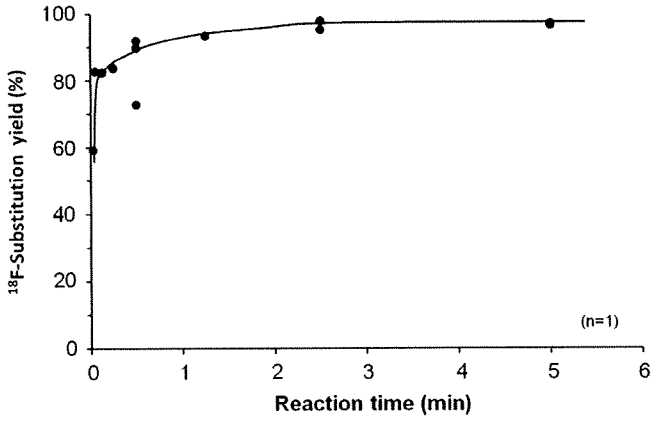

Fig. 9. Correlation between ^{18}F-substitution of mannose triflate and reaction time at 80 °C in microfluidic setup.

[^{18}F]fluoride remained after the release and transfer process and the remaining ^{18}F was washed out with water.

More than one preparation of anhydrous [K^+/K.222]$^{18}F^-$ solution can be produced by repeating the concentration process using the same disposable flow cell. The cell could be re-used up to 10 times, although a relatively large variation in both deposition (81–91%, n=8) and overall recovery (42–69%, n=8) was observed. Thus, simply washing the cell with water conveniently allows repetition of the preparation within a short time interval. However, black residues, possibly derived from the GC plate, were seen during washings and this suggests decomposition of the GC surface resulting in lower efficiency and leading to a limitation in use.

3.4. *Reactivity of the recovered [^{18}F]fluoride*

Using the concentrated [K^+/K.222]$^{18}F^-$ solution protected [^{18}F]FDG was obtained in high radiochemical yields (> 80%) by the conventional ^{18}F-fluorination. This result encouraged us to proceed to microfluidic radiosynthesis of [^{18}F]FDG to demonstrate the feasibility of the electrochemically concentrated solution of [K^+/K.222]$^{18}F^-$ in microfluidics. The correlation between ^{18}F-substitution yield and reaction time shows that only 3 s is enough for ^{18}F-substitution yields of over 80% and 30 s for over 90% (Fig. 9). This high-speed reaction is probably due to efficient mixing and heat transfer in microchannels as often emphasized in microfluidic reactions (Wester et al., 2009). The reaction was completed within 2 min when starting at a flow rate of 100 μL/min from a 100 μL solution of [K^+/K.222]$^{18}F^-$ in the transfer loop. The results suggest that the [^{18}F]fluoride solution provided by the present method has high reactivity towards substitution reactions.

4. Conclusions

The present study showed that n.c.a. [^{18}F]fluoride dissolved in target water can be concentrated into a MeCN solution containing K.222–$KHCO_3$ in overall efficiencies above 60% by electrochemical deposition and release on a disposable microfluidic cell. The automated module can provide highly reactive [K^+/K.222]$^{18}F^-$ in 60 μL of MeCN within 6 min. High reactivity of the [K^+/K.222]$^{18}F^-$ was demonstrated in the radiosynthesis of [^{18}F]FDG on a microfluidic reactor.

Acknowledgments

This study was partly supported by a Grant-in-Aid (No. 19390311) for Scientific Research (B) from the Japan Society for the Promotion of Science.

Reference

Alexoff, D., Schlyer, D.J., Wolf, A.P., 1989. Recovery of [^{18}F]fluoride from [^{18}O]water in an electrochemical cell. Appl. Radiat. Isot. 40, 1–6.

Gillies, J.M., Prenant, C., Chimon, G.N., Smethurst, G.J., Perrie, W., Hamblett, I., Dekker, B., Zweit, J., 2006a. Microfluidic reactor for the radiosynthesis of PET tracers. Appl. Radiat. Isot. 64, 325–332.

Gillies, J.M., Prenant, C., Chimon, G.N., Smethurst, G.J., Dekker, B., Zweit, J., 2006b. Microfluidic technology for PET radiochemistry. Appl. Radiat. Isot. 64, 333–336.

Hamacher, K., Blessing, G., 1995. Process for separating carrier-free radionuclides from target liquid. Its use and arrangement therefor. PCT WO 1995/18668.

Hamacher, K., Coenen, H.H., Stöcklin, G., 1986. Efficient stereospecific synthesis of no-carrier-added 2-[^{18}F]-fluoro-2-deoxy-D-glucose using aminopolymer supported nucleophilic substitution. J. Nucl. Med. 27, 235–238.

Hamacher, K., Coenen, H.H., 2006. No-carrier-added nucleophilic ^{18}F-labelling in an electrochemical cell exemplified by the routine production of [^{18}F]altanserin. Appl. Radiat. Isot. 64, 989–994.

Hamacher, K., Hirschfelder, T., Coenen, H.H., 2002. Electrochemical cell for separation of [^{18}F]fluoride from irradiated ^{18}O-water and subsequent no carrier added nucleophilic fluorination. Appl. Radiat. Isot. 56, 519–523.

Ido, T., Wan, C.N., Cassela, V., Fowler, J.S., Wolf, A.P., 1978. Labeled 2-deoxy-D-glucose analogs. ^{18}F-Labeled 2-deoxy-2-fluoro-D-glucose, 2-deoxy-2-fluoro-D-mannose and ^{14}C-2-deoxy- 2-fluoro-D-glucose. J. Label. Compd. Radiopharm. 14, 175–183.

Lee, C.-C., Sui, G., Elizarov, A., Shu, C.J., Shin, Y.-S., Dooley, A.N., Huang, J., Daridon, A., Wyatt, P., Stout, D., Kolb, H.C., Witte, O.N., Satyamurthy, N., Heath, J.R., Phelps, M.E., Quake, S.R., Tseng, H.-R., 2005. Multistep synthesis of a radiolabeled imaging probe using integrated microfluidics. Science 310, 1793–1796.

Liow, E., O'Brien, A., Luthra, S., Brady, F., 2005. Preliminary studies of conducting high level production radiosyntheses using microfluidic device. J. Label. Compd. Radiopharm. 48, S28.

Reischl, G., Ehrlichmann, W., Machulla, H.-J., 2002. Electrochemical transfer of [^{18}F]fluoride from [^{18}O]water into organic solvents ready for labeling reactions. J. Radioanal. Nucl. Chem. 254, 29–31.

Rensch, C., Boeld, C., Bachmann, B., Reischel, G., Ehrlichmann, W., Heumesser, N., Baller, M., Samper, V., 2009. Microfluidic radiosynthesis: electrochemical phase transfer dor drying [^{18}F]fluoride. J. Label. Compd. Radiopharm. 52, S8.

Saiki, H., Iwata, R., Wong, R., Furumoto, S., Ishikawa, Y., Nakanishi, H., Ozeki, E., 2009. Electrochemical concentration of aqueous [^{18}F]fluoride into an aprotic solvent in a disposable microfluidic cell. J. Label. Compd. Radiopharm. 52, S505.

Schlyer, D.J., Bastos, M.A.V., Alexoff, D., Wolf, A.P., 1990. Separation of [^{18}F]fluoride from [^{18}O]water using anion exchange resin. Appl. Radiat. Isot. 41, 531–533.

Wester, H.-J., Schoultz, B.W., Hultsch, C., Henriksen, G., 2009. Fast and repetitive in-capillary production of [^{18}F]FDG. Eur. J. Nucl. Med. Mol. Imaging 36, 653–658.

Please cite this article as: Saiki, H., et al., Electrochemical concentration of no-carrier-added [^{18}F]fluoride from [^{18}O]water in a disposable microfluidic cell for radiosynthesis of ^{18}F-labeled radiopharmaceuticals. Appl. Radiat. Isotopes (2010), doi:10.1016/j.apradiso.2010.02.005

Original Article

Effect of Exercise Intervention on Endothelial Function and Incidence of Cardiovascular Disease in Patients with Type 2 Diabetes

Sadanori Okada[1], Aki Hiuge[1], Hisashi Makino[1], Ayako Nagumo[1], Hiroshi Takaki[2], Harumi Konishi[3], Yoichi Goto[4], Yasunao Yoshimasa[1], Yoshihiro Miyamoto[1]

[1]Department of Atherosclerosis and Diabetes, National Cardiovascular Center, Osaka, Japan
[2]Department of Cardiovascular Dynamics, National Cardiovascular Center Institute, Osaka, Japan
[3]Department of Rehabilitation, National Cardiovascular Center, Osaka, Japan
[4]Department of Cardiology, National Cardiovascular Center, Osaka, Japan

Background: The effects of exercise intervention and its long-term efficacy in preventing subsequent cardiovascular events in patients with type 2 diabetes have been little studied in randomized controlled trials. ***Methods and Results***: Thirty-eight type 2 diabetic patients (21 men and 17 women) were assigned to either the exercise group ($n=21$) or the control group without exercise training ($n=17$) by simple randomization. The exercise training group was scheduled for aerobic and resistance exercise programs for 3 months, after which we investigated endothelial function, insulin resistance, adipocytokines and inflammatory markers. Endothelial function was evaluated by examining flow-mediated endothelium-dependent vasodilatation (FMD). Furthermore, we followed the incidence of cardiovascular events for 24 months. After 3 months, HbA1c decreased significantly in both groups, and FMD increased from 7.3±4.7% to 10.9±6.2% only in the exercise group ($p<0.05$). Long-term follow-up data showed that the control group developed cardiovascular events more frequently than did the exercise group ($p<0.05$). ***Conclusions***: Exercise improves endothelial dysfunction independently of glycemic control and insulin sensitivity in patients with type 2 diabetes. The beneficial effects of 3-month exercise to reduce cardiovascular events persist for 24 months.

J Atheroscler Thromb, 2010; 17:000-00.

Key words; Exercise, Type 2 diabetes, Endothelial function, Cardiovascular events

Introduction

Physical exercise has been reported to reduce the incidence of diabetes[1, 2], and its modification has long been recommended as one of the three main components of diabetic treatments in addition to diet modification and medication[3]. It is well known that regular exercise produces beneficial effects on risk factors of atherosclerosis by improving glycemic control[4], insulin resistance[5], and dyslipidemia and hypertension[6], and contributes to reduce cardiovascular morbidity and mortality not only in the general population[7, 8] but also in patients with type 2 diabetes[9, 10]; however, the mechanisms by which exercise training prevents the progression of atherosclerotic diseases in type 2 diabetes are still unclear, and the effect of exercise on the prognosis of patients with type 2 diabetes remains uncertain.

The purpose of the present study was to investigate the effects of exercise intervention on endothelial function, insulin resistance, adipocytokines and inflammatory markers in patients with type 2 diabetes in a randomized controlled trial. To assess the long-term efficacy of exercise intervention on the prevention of atherosclerotic disorders, we examined the follow-up data of the participants after the exercise intervention period.

Address for correspondence: Yoshihiro Miyamoto M.D., Ph.D., Department of Atherosclerosis and Diabetes, National Cardiovascular Center, 5-7-1 Fujishirodai, Suita, Osaka 565-8565, Japan.
E-mail: miyamoty@hsp.ncvc.go.jp
Received:
Accepted for publication:

Methods

Study subjects and intervention protocol

Thirty-eight Japanese patients (21 men and 17 women) with type 2 diabetes, who were admitted to our hospital for treatment of diabetes from August 2002 to January 2004, participated in this study. Patients who had symptomatic coronary artery disease, proliferative diabetic retinopathy, overt proteinuria, autonomic disorder or orthopedic disorders were excluded from this study. The study design was approved by the ethics committee of the National Cardiovascular Center. All participants gave written informed consent.

Study participants were assigned to either the exercise training group (exercise group, $n=21$) or the group without exercise training (control group, $n=17$) by simple randomization without the permuted block method. Patients in the exercise group were scheduled for exercise programs 3–5 times weekly for 3 months, supervised by physiotherapists. Each session consisted of 10-min warming-up, 20-min aerobic dance, 20-min stationary bicycle riding, 20-min resistance training and 5-min cool-down. The training heart rate was determined according to Karvonen's equation ($k=0.6$)[11]. Patients in the control group did not take part in the exercise programs. Both groups received comparable dietary and medical intervention after registration for 3 months.

Clinical examination and measurement of exercise capacity and insulin sensitivity

Clinical and metabolic parameters, including exercise capacity and insulin sensitivity, were measured before and after the intervention period. Systolic and diastolic blood pressures were examined after a minimum of 10-min rest in a sitting position. Body mass index (BMI) was calculated as weight in kilograms divided by the square of the height in meters. Blood samples were collected in the morning after a 12-hour overnight fast, and fasting plasma glucose, HbA1c, lipid profiles, serum adiponectin, leptin, and high-sensitivity C-reactive protein (CRP) levels were analyzed. Exercise capacity was determined by cardiopulmonary exercise testing, the details of which have been published elsewhere[11]. Insulin sensitivity was evaluated by the modified steady-state plasma glucose method (SSPG)[12].

Assessment of endothelial function by flow-mediated brachial artery dilatation

Endothelial function was studied by examining the brachial artery response to flow-mediated endothelium-dependent vasodilatation (FMD), according to the method described previously[13]. Briefly, participants were examined after 15-min rest in the fasting state. After baseline diameter of the right brachial artery was measured by ultrasound images, the pneumatic cuff placed around the right forearm was inflated to 220 mmHg to occlude the brachial artery. The cuff was kept inflated for 270 seconds, and then the diameter of the brachial artery was measured for 120 seconds after cuff deflation. FMD was calculated from baseline and maximum diameters of the brachial artery.

Long-term follow-up of clinical events of the diabetic patients

As a post-hoc study, most of the participants (exercise group, $n=21$; control group, $n=17$) were followed in our outpatient unit for 24 months after randomization. We accumulated the follow-up data for 24 months and determined new-onset cardiovascular events, including acute myocardial infarction, angina pectoris, cerebral infarction, and cerebral hemorrhage.

Statistical analysis

Analysis was based on the intention-to-treat principle. Data was expressed as the means ± S.D. To compare the two groups, we used two-tailed unpaired t tests for continuous variables. The differences between the baseline and after 3 months were evaluated by the two-tailed paired t test in each group. Additionally, we analyzed the incidence of cardiovascular events during 24 months after randomization by Kaplan-Meier analysis of the time to cardiovascular events according to exercise intervention. All analysis was conducted using JMP version 6.0 software (SAS Institute Inc., USA). *p values* below 0.05 were considered statistically significant.

Results

The clinical backgrounds of the two groups are shown in **Table 1**. The clinical and metabolic parameters at baseline except for SSPG were not significantly different between the two groups (**Table 2**), while SSPG at baseline in both groups indicated an insulin-resistant state. After the 3-month intervention, HbA1c and serum LDL cholesterol levels were decreased and serum HDL cholesterol and serum adiponectin levels were increased in both groups. BMI was significantly decreased and peak $\dot{V}O_2$ and FMD were significantly increased only in the exercise group. SSPG was significantly decreased only in the control group. Serum leptin levels were increased only in the control group.

Table 1. Clinical backgrounds of the exercise and control groups

	Exercise group ($n=21$)	Control group ($n=17$)	p
Men/Women	10/11	11/6	0.290
Age (year)	61.9 ± 8.6	64.5 ± 5.9	0.293
Duration of diabetes (year)	9.5 ± 8.1	10.8 ± 7.4	0.52
Previous coronary artery diseases, *n* (%)	9 (42.9)	9 (52.9)	0.536
Current smoker, *n* (%)	4 (19.0)	2 (11.8)	0.536
Therapy for diabetes at baseline, *n* (%)			
Diet only	8 (38.1)	3 (17.7)	0.167
Insulin	3 (14.3)	3 (17.6)	0.778
Sulfonylurea or Glinide	6 (28.6)	7 (41.2)	0.415
Biguanide	5 (23.8)	7 (41.2)	0.252
Thiazolidindione	0 (0)	0 (0)	-
α-glucosidase inhibitor	4 (19.1)	6 (35.3)	0.258
Therapy for diabetes after 3 months, *n* (%)			
Diet only	12 (57.1)	3 (17.7)	0.013
Insulin	1 (4.8)	3 (17.7)	0.198
Sulfonylurea or Glinide	4 (19.1)	7 (41.2)	0.135
Biguanide	5 (23.8)	6 (35.3)	0.438
Thiazolidindione	0 (0)	0 (0)	-
α-glucosidase inhibitor	4 (19.1)	8 (47.1)	0.065
Other medications at baseline, *n* (%)			
β-blockers	5 (23.8)	7 (41.2)	0.252
ACE inhibitors/ARBs	9 (42.9)	3 (17.6)	0.096
Statins	7 (33.3)	6 (35.3)	0.899
Other medications after 3 months, *n* (%)			
β-blockers	4 (19.1)	7 (41.2)	0.134
ACE inhibitors/ARBs	11 (52.4)	3 (17.6)	0.027
Statins	7 (33.3)	8 (47.1)	0.389

Data are the means ± S.D. ACE, angiotensin II converting enzyme; ARB, angiotensin II type 1 receptor blocker

Table 2. Effects of exercise training on clinical and metabolic values

	Exercise group ($n=21$)		Control group ($n=17$)	
	Baseline	After 3 months	Baseline	After 3 months
BMI (kg/m^2)	25.7 ± 3.2	25.3 ± 3.4*	24.5 ± 2.9	23.9 ± 2.6
SBP (mmHg)	129.0 ± 21.6	130.5 ± 18.6	126.6 ± 16.8	130.4 ± 16.1
DBP (mmHg)	74.6 ± 11.6	78.5 ± 11.7	73.8 ± 11.8	76.3 ± 13.3
Peak $\dot{V}O_2$/kg (mL/kg/min)	22.4 ± 3.2	24.4 ± 3.8*	22.3 ± 3.7	24.0 ± 4.4
Basal Diameter (mm)	3.90 ± 0.78	3.88 ± 0.75	3.91 ± 0.71	4.19 ± 0.76
FMD (%)	7.3 ± 4.7	10.9 ± 6.2**	6.4 ± 3.6	7.4 ± 5.0
ND (%)	14.5 ± 6.3	12.6 ± 5.1	9.8 ± 5.6	12.3 ± 7.0
FPG (mmol/L)	7.7 ± 2.0	8.1 ± 2.4	8.2 ± 1.6	7.5 ± 1.7
HbA_{1C} (%)	8.5 ± 1.8	7.0 ± 1.3**	7.9 ± 1.1	6.8 ± 0.8**
SSPG (mmol/L)	11.1 ± 5.3	9.7 ± 4.2	14.1 ± 3.4	9.7 ± 4.6**
Total cholesterol (mmol/L)	5.28 ± 0.95	4.84 ± 0.74	5.11 ± 1.45	4.46 ± 0.09*
Triglyceride (mmol/L)	1.67 ± 1.55	1.37 ± 0.70	1.35 ± 0.67	1.34 ± 1.41
HDL cholesterol (mmol/L)	1.17 ± 0.22	1.33 ± 0.36**	1.23 ± 0.26	1.35 ± 0.28*
LDL cholesterol (mmol/L)	3.34 ± 0.64	2.88 ± 0.79**	3.26 ± 1.25	2.50 ± 0.74*
Leptin (pg/mL)	5.3 ± 3.1	6.5 ± 3.5	5.2 ± 5.0	6.6 ± 4.9*
Adiponectin (ng/mL)	6.1 ± 3.3	8.0 ± 4.3**	5.3 ± 2.4	7.1 ± 3.7**
high-sensitivity CRP (ng/mL)	1292.6 ± 1843.4	1178.8 ± 1680.5	841.6 ± 738.0	814.2 ± 1257.0

Data are the means ± S.D. *$p<0.05$, Baseline vs. after 3 months in each group. **$p<0.01$, Baseline vs. after 3 months in each group. BMI, body mass index; SBP, systolic blood pressure; DBP, diastolic blood pressure; FMD, flow-mediated endothelium-dependent vasodilatation; ND, nitroglycerin-induced vasodilatation; FPG, fasting plasma glucose; SSPG, steady state plasma glucose; CRP, C-reactive protein.

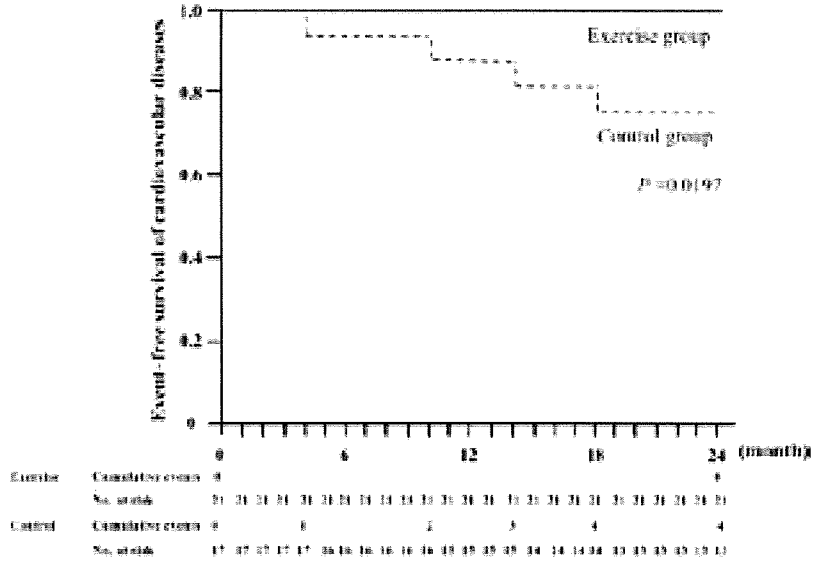

Fig. Kaplan-Meier analysis of the time to a cardiovascular event according to exercise intervention

The 38 patients were followed up until 24 months after randomization. In the control group, 1 patient developed angina pectoris and 3 patients developed cerebral infarction. On the other hand, patients in the exercise group had no cardiovascular events ($p=0.0197$).

There were no significant changes in high-sensitivity CRP levels in both groups.

Thirty-two of the 38 patients (exercise group: $n=16$, control group: $n=16$) were followed up until 24 months after randomization. We could not follow up 5 patients in the exercise group and 1 patient in the control group, because they went to other clinics after the 3-month intervention period. In the control group, 1 patient developed angina pectoris and 3 patients developed cerebral infarction. On the other hand, patients in the exercise group had no cardiovascular events (**Fig.**).

Discussion

The present study demonstrated that exercise intervention improved FMD, a surrogate marker of endothelial function, in patients with type 2 diabetes. Moreover, the 24-month follow-up study showed that the 3-month exercise intervention prevented new-onset cardiovascular events.

This study was a randomized controlled study of exercise treatment and was analyzed by intention-to-treat. Medications for diabetes, hypertension and dyslipidemia were provided to both groups comparably. Patients using insulin and sulfonylurea usage decreased and those with diet alone increased in the exercise group. These changes in medication might have affected the results of metabolic parameters.

Patients with type 2 diabetes have a greater incidence of cardiovascular diseases than non-diabetic patients[14], and they often have endothelial dysfunction[15, 16]. Vascular endothelium plays an important role in the control of vascular tone, and endothelial dysfunction is considered to be an early manifestation of the atherosclerotic process[17]. Several clinical studies have demonstrated that exercise intervention corrects endothelial dysfunction not only in healthy individuals[18] but also in patients with coronary artery disease[19]. A recent study has shown that exercise training improves the indices of glycemic control and endothelial dysfunction in patients with type 2 diabetes[20]; however, it is unclear whether the amelioration of endothelial dysfunction is independent of glycemic control, because HbA1c is reported to inversely correlate with FMD[21]. In our study, HbA1c was improved in both groups after the 3-month intervention period regardless of exercise training, and SSPG was not significantly improved by exercise intervention. These data suggest that alterations in HbA1c or SSPG levels may not account for the improvement of FMD, implying that physical exercise has a beneficial impact on endothelial function beyond glycemic control and insulin sensitivity.

Moreover, our 24-month follow-up study showed that the 3-month exercise intervention prevented new-onset cardiovascular events. Few previous studies have investigated the effect of exercise intervention on long-term outcomes in terms of cardiovascular events in a randomized control trial. A previous report suggested that endothelial dysfunction precedes atherosclerosis and future cardiovascular events[22], and our study supports the relevance of short-term exercise intervention in the management of type 2 diabetes, albeit perhaps only for a certain period.

We also investigated the effect of physical exercise on adipocytokines: adiponectin and leptin. Adiponectin plays an important role in inducing insulin resistance and atherosclerosis[23], and several studies concerning the effect of physical exercise on serum adiponectin levels have yielded inconsistent findings[5, 24, 25]. Our study showed that serum adiponectin levels were increased in both groups. This result may imply that serum adiponectin is increased by the improvement of glycemic control, regardless of exercise intervention or weight reduction. An anti-diabetic agents, thiazolidinedione, has been reported to increase plasma adiponectin levels[26, 27], but no patients took thiazolidinediones in our study. Serum leptin levels are positively correlated with total body adiposity[28] and are reported to decrease with weight reduction[29], but it is controversial whether exercise training decreases serum leptin levels without reduction of body fat mass[24, 30]. In our study, serum leptin levels were not changed in the exercise group and increased in the control group, whereas body weight was decreased only in the exercise group. Patients in the control group might have much less lean body mass than those in the exercise group, but further investigation is needed to settle this issue.

Chronic inflammation is thought to present as an early sign of atherosclerosis[31]. Previous studies have demonstrated that regular physical exercise is associated with low serum CRP levels and exercise intervention reduces serum CRP levels[32]. In the present study, serum high-sensitivity CRP levels were not altered in either group. Since serum CRP levels are influenced by various pro-inflammatory and inflammatory factors and the number of participants in our study was limited, it is difficult to conclude whether exercise intervention affects serum CRP levels.

Our study has several limitations. First, since we had no information on physical activity during the follow-up period, we could not exclude the possibility that the extent of physical exercise affects the prevention of cardiovascular events. Second, the persistence of the increased FMD in the exercise group was unclear, and the amelioration of endothelial dysfunction could not be comfirmed as the major mechanism of the prevention of cardiovascular events in this study. Third, the improvement of endothelial function might have been affected by the exercise group having a higher prevalence of taking angiotensin-converting enzyme inhibitors or angiotensin II receptor blockers at baseline and after 3 months.

In conclusion, our study demonstrates that exercise intervention has beneficial effects on endothelial function in patients with type 2 diabetes. Our findings also suggest that exercise training exerts anti-atherosclerotic effects independently of glycemic control and insulin sensitivity. Finally, the favorable effects of a 3-month exercise intervention to reduce cardiovascular events may persist for up to 24 months, although further study is necessary for confirm this.

Acknowledgements

We express our gratitude to Ms. Chie Kobayashi and Ms. Keiko Toda for their support of our study. We also express our thanks to Ms. Akiko Kada for her advice on statistical analysis. This study was supported by a Research Grant for Cardiovascular Disease from the Ministry of Health, Labour and Welfare.

References

1) Tuomilehto J, Lindström J, Eriksson JG, Valle TT, Hämäläinen H, Ilanne-Parikka P, Keinänen-Kiukaanniemi S, Laakso M, Louheranta A, Rastas M, Salminen V, Uusitupa M; Finnish Diabetes Prevention Study Group: Prevention of type 2 diabetes mellitus by changes in lifestyle among subjects with impaired glucose tolerance. N Engl J Med, 2001; 344: 1343-1350
2) Knowler WC, Barrett-Connor E, Fowler SE, Hamman RF, Lachin JM, Walker EA, Nathan DM; Diabetes Prevention Program Research Group: Reduction in the incidence of type 2 diabetes with lifestyle intervention or metformin. N Engl J Med, 2002; 346: 393-403
3) Sigal RJ, Kenny GP, Wasserman DH, Castaneda-Sceppa C, White RD: Physical activity/exercise and type 2 diabetes: a consensus statement from the American Diabetes Association. Diabetes Care, 2006; 29: 1433-1438
4) Boule NG, Haddad E, Kenny GP, Wells GA, Sigal RJ: Effects of exercise on glycemic control and body mass in type 2 diabetes mellitus: a meta-analysis of controlled clinical trials. JAMA, 2001; 286: 1218-1227
5) Yokoyama H, Emoto M, Araki T, Fujiwara S, Motoyama K, Morioka T, Koyama H, Shoji T, Okuno Y, Nishizawa Y: Effect of aerobic exercise on plasma adiponectin levels and insulin resistance in type 2 diabetes. Diabetes Care, 2004; 27: 1756-1758
6) Balducci S, Leonetti F, Di Mario U, Fallucca F: Is a long-term aerobic plus resistance training program feasible for

and effective on metabolic profiles in type 2 diabetic patients? Diabetes Care, 2004; 27: 841-842
7) Hakim AA, Petrovitch H, Burchfiel CM, Ross GW, Rodriguez BL, White LR, Yano K, Curb JD, Abbott RD: Effects of walking on mortality among nonsmoking retired men. N Engl J Med, 1998; 338: 94-99
8) Bijnen FC, Caspersen CJ, Feskens EJ, Saris WH, Mosterd WL, Kromhout D: Physical activity and 10-year mortality from cardiovascular diseases and all causes: The Zutphen Elderly Study. Arch Intern Med, 1998; 158: 1499-1505
9) Wei M, Gibbons LW, Kampert JB, Nichaman MZ, Blair SN: Low cardiorespiratory fitness and physical inactivity as predictors of mortality in men with type 2 diabetes. Ann Intern Med, 2000; 132: 605-611
10) Hu FB, Stampfer MJ, Solomon C, Liu S, Colditz GA, Speizer FE, Willett WC, Manson JE: Physical activity and risk for cardiovascular events in diabetic women. Ann Intern Med, 2001; 134: 96-105
11) Uchida I, Takaki H, Kobayashi Y, Okano Y, Satoh T, Matsubara T, Goto Y: O2 extraction during exercise determines training effect after cardiac rehabilitation in myocardial infarction. Circ J, 2002; 66: 891-896
12) Suzuki M, Kimura Y, Tsushima M, Harano Y: Association of insulin resistance with salt sensitivity and nocturnal fall of blood pressure. Hypertension, 2000; 35: 864-868
13) Suzuki M, Takamisawa I, Suzuki K, Hiuge A, Horio T, Yoshimasa Y, Harano Y: Close association of endothelial dysfunction with insulin resistance and carotid wall thickening in hypertension. Am J Hypertens, 2004; 17: 228-232
14) Kannel WB, McGee DL: Diabetes and cardiovascular disease. The Framingham study. JAMA, 1979; 241: 2035-2038
15) Calver A, Collier J, Vallance P: Inhibition and stimulation of nitric oxide synthesis in the human forearm arterial bed of patients with insulin-dependent diabetes. J Clin Invest, 1992; 90: 2548-2554
16) Tsuchiya K, Nakayama C, Iwashima F, Sakai H, Izumiyama H, Doi M, Hirata Y: Advanced endothelial dysfunction in diabetic patients with multiple risk factors; importance of insulin resistance. J Atheroscler Thromb, 2007; 14: 303-309
17) Landmesser U, Hornig B, Drexler H: Endothelial function: a critical determinant in atherosclerosis? Circulation, 2004; 109: II27-II33
18) Clarkson P, Montgomery HE, Mullen MJ, Donald AE, Powe AJ, Bull T, Jubb M, World M, Deanfield JE: Exercise training enhances endothelial function in young men. J Am Coll Cardiol, 1999; 33: 1379-1385
19) Hambrecht R, Wolf A, Gielen S, Linke A, Hofer J, Erbs S, Schoene N, Schuler G: Effect of exercise on coronary endothelial function in patients with coronary artery disease. N Engl J Med, 2000; 342: 454-460
20) Maiorana A, O'Driscoll G, Cheetham C, Dembo L, Stanton K, Goodman C, Taylor R, Green D: The effect of combined aerobic and resistance exercise training on vascular function in type 2 diabetes. J Am Coll Cardiol, 2001; 38: 860-866
21) Mäkimattila S, Virkamäki A, Groop PH, Cockcroft J, Utriainen T, Fagerudd J, Yki-Järvinen H: Chronic hyperglycemia impairs endothelial function and insulin sensitivity via different mechanisms in insulin-dependent diabetes mellitus. Circulation, 1996; 94: 1276-1282
22) Suwaidi JA, Hamasaki S, Higano ST, Nishimura RA, Holmes DR, Jr., Lerman A: Long-term follow-up of patients with mild coronary artery disease and endothelial dysfunction. Circulation, 2000; 101: 948-954
23) Ritchie SA, Ewart MA, Perry CG, Connell JM, Salt IP: The role of insulin and the adipocytokines in regulation of vascular endothelial function. Clin Sci (Lond), 2004; 107: 519-532
24) Monzillo LU, Hamdy O, Horton ES, Ledbury S, Mullooly C, Jarema C, Porter S, Ovalle K, Moussa A, Mantzoros CS: Effect of lifestyle modification on adipokine levels in obese subjects with insulin resistance. Obes Res, 2003; 11: 1048-1054
25) Boudou P, Sobngwi E, Mauvais-Jarvis F, Vexiau P, Gautier JF: Absence of exercise-induced variations in adiponectin levels despite decreased abdominal adiposity and improved insulin sensitivity in type 2 diabetic men. Eur J Endocrinol, 2003; 149: 421-424
26) Yang WS, Jeng CY, Wu TJ, Tanaka S, Funahashi T, Matsuzawa Y, Wang JP, Chen CL, Tai TY, Chuang LM: Synthetic peroxisome proliferator-activated receptor-gamma agonist, rosiglitazone, increases plasma levels of adiponectin in type 2 diabetic patients. Diabetes Care, 2002; 25: 376-380
27) Miyazaki Y, Mahankali A, Wajcberg E, Bajaj M, Mandarino LJ, DeFronzo RA: Effect of pioglitazone on circulating adipocytokine levels and insulin sensitivity in type 2 diabetic patients. J Clin Endocrinol Metab, 2004; 89: 4312-4319
28) Considine RV, Sinha MK, Heiman ML, Kriauciunas A, Stephens TW, Nyce MR, Ohannesian JP, Marco CC, McKee LJ, Bauer TL, José FC: Serum immunoreactive-leptin concentrations in normal-weight and obese humans. N Engl J Med, 1996; 334: 292-295
29) Xenachis C, Samojlik E, Raghuwanshi MP, Kirschner MA: Leptin, insulin and TNF-alpha in weight loss. J Endocrinol Invest, 2001; 24: 865-870
30) Pasman WJ, Westerterp-Plantenga MS, Saris WH: The effect of exercise training on leptin levels in obese males. Am J Physiol, 1998; 274: E280-E286
31) Ross R: Atherosclerosis--an inflammatory disease. N Engl J Med, 1999; 340: 115-126
32) Kasapis C, Thompson PD: The effects of physical activity on serum C-reactive protein and inflammatory markers: a systematic review. J Am Coll Cardiol, 2005; 45: 1563-1569

DOI: 10.3171/2010.3.JNS091057

Assessment of necrotic core with intraplaque hemorrhage in atherosclerotic carotid artery plaque by MR imaging with 3D gradient-echo sequence in patients with high-grade stenosis

Clinical article

TOMOHITO HISHIKAWA, M.D.,[1] KOJI IIHARA, M.D.,[1] NAOAKI YAMADA, M.D.,[2] HATSUE ISHIBASHI-UEDA, M.D.,[3] AND SUSUMU MIYAMOTO, M.D.[1]

Departments of [1]Neurosurgery, [2]Radiology, and [3]Pathology, National Cardiovascular Center, Osaka, Japan

Object. The aim of this study was to assess the histopathological differences between advanced atherosclerotic carotid artery (CA) plaques with signal hyperintensity on T1-weighted MR images and those without, focusing on necrotic core size and intraplaque hemorrhage (IPH).

Methods. Thirty-five patients scheduled for carotid endarterectomy underwent preoperative CA MR imaging using 3D inversion-recovery-based T1-weighted imaging (magnetization-prepared rapid acquisition gradient-echo [MPRAGE]). The signal intensity of the CA plaque on MPRAGE sequences was classified as "high" when the intensity was more than 200% that of adjacent muscle. A total of 96 axial MR images obtained in 35 patients were compared with corresponding histological sections from 36 excised specimens. The area of the necrotic core in histological sections was compared between specimens with and without high signal intensity on MPRAGE sequences. The IPH was histopathologically graded according to the size of the area positive for glycophorin A as revealed by immunohistochemical staining. The difference between plaques with and without high signal intensity was investigated with respect to the degree of IPH. The relationship of the severity of IPH to size of the necrotic core was also evaluated.

Results. The area of the necrotic core in plaques with high signal intensity on MPRAGE sequences was significantly larger than that in plaques without high signal intensity (median 51.2% [interquartile range 43.3–66.8%] vs 49.0% [33.2–57.6%], $p = 0.029$). Carotid artery plaques with high signal intensity had significantly more severe IPH than plaques with lower signal intensity ($p < 0.0001$). The severity of IPH was significantly associated with the size of the necrotic core ($p < 0.0001$).

Conclusions. Atherosclerotic CA plaques with high signal intensity on MPRAGE sequences had large necrotic cores with IPH in patients with high-grade stenosis; MPRAGE is useful for the evaluation of CA plaque progression. *(DOI: 10.3171/2010.3.JNS091057)*

KEY WORDS • carotid artery stenosis • intraplaque hemorrhage • MR imaging • necrotic core

THE prophylactic effectiveness of CEA in patients with more than a certain degree of arterial stenosis has been proven in several randomized multicenter trials.[7,8,11,21] Although the degree of lumen narrowing is a significant risk factor in stroke, the role of vulnerable CA plaque has recently been emphasized,[20] and some reports have demonstrated that episodes of cerebral ischemia in patients with CA lesions are not restricted to cases with severe stenosis.[3,10,24] The type of vulnerable plaque that is most prone to rupture is characterized by a large necrotic core, a thin fibrous cap (< 65 μm thick), and widespread macrophage infiltration within the fibrous cap.[31] In addition, the role of IPH in the vulnerability of CA plaques has been emphasized by many investigators.[6,17,26,28,29,34]

Magnetic resonance imaging is well suited for CA plaque evaluation in a clinical setting because it is noninvasive and widely available, provides excellent soft tissue contrast, and does not involve ionizing radiation. In response to reports demonstrating the close association of IPH with cerebral ischemic events,[26] many authors have recently emphasized the value of IPH detection by MR imaging and have demonstrated the clinical usefulness of this noninvasive modality.[1,6,13,17,28,29,33]

Our institute has routinely performed CA plaque MR imaging using 3D inversion-recovery-based T1-weighted sequences (MPRAGE) before interventions for CA stenosis. Yamada et al.[33] demonstrated that CA plaque with high signal intensity on MPRAGE sequences was significantly associated with previous ipsilateral ischemic events in patients with moderate and severe stenosis. In that report,

Abbreviations used in this paper: CA = carotid artery; CEA = carotid endarterectomy; ICA = internal carotid artery; IPH = intraplaque hemorrhage; IQR = interquartile range; MPRAGE = magnetization-prepared rapid acquisition gradient echo.

This article contains some figures that are displayed in color online but in black and white in the print edition.

CA plaque signal intensity on greater than 200% that of adjacent muscles was defined as high and the chi values for interobserver and intraobserver agreement were 0.729 and 0.792, respectively (good agreement).[33] Taking the close association of MPRAGE signal intensity (using a threshold of 200% of the intensity of adjacent muscles) with symptomatology into consideration, we sought to determine the histopathological differences between CA plaques with and without high signal intensity as the next stage of investigation. The aim of this study was to retrospectively assess the vulnerability of CA plaques, focusing on differences in necrotic core area and degree of IPH between plaques that are associated with high signal intensity on MPRAGE sequences and those that are associated with lower signal intensity (< 200% of the intensity of adjacent muscle tissue).

Methods

Study Population

Thirty-five patients (32 men, 3 women) with a mean (± SD) age of 69.0 ± 7.8 years who were scheduled for CEA at our institute between May 2006 and March 2007 were included in this study. Patient characteristics were examined retrospectively through a review of the relevant medical records. A total of 36 CEAs for CA stenosis (1 patient had bilateral CA stenosis) were performed, and 36 endarterectomy specimens were analyzed. Twenty patients (57.1%) had a history of ipsilateral ischemic events, including cerebral infarction, transient ischemic attack, and retinal ischemia, within the previous 6 months, and their lesions were defined as symptomatic. The degree of CA stenosis was measured using digital subtraction angiography (17 lesions), 3D CT angiography (17 lesions), or contrast-enhanced MR angiography (2 lesions) according to the method used in the North American Symptomatic Carotid Endarterectomy Trial (NASCET).[9] The criteria for CEA were 70% stenosis or greater for symptomatic cases and 75% stenosis or greater for asymptomatic cases.[12] All 36 endarterectomy specimens were circumferentially removed with the plaque intact.

Magnetic Resonance Imaging Protocol

Imaging was performed using standard neck array and spine array coils in a Magnetom Sonata 1.5-T system (Siemens). Plaque imaging was performed using MPRAGE in the transaxial section with null blood condition (effective inversion time 660 msec; TR 1500 msec) and the water excitation technique to suppress fat signals.[33] Other scanning parameters were as follows: TE 5.0 msec; FOV 180 × 180 mm; matrix 256 × 204; section thickness 1.25 mm; 56 partitions, covering 70 mm around the CA bifurcation; and data acquisition time 5 minutes. The mean interval between MR imaging and CEA was 17.9 ± 20.4 days. In symptomatic patients, the mean duration of time from last symptoms to MR imaging was 16.2 ± 27.0 days.

Image Review and Criteria

The MR images were reviewed by an experienced radiologist (N.Y.) blinded to clinical and pathological data. The signal intensity of plaques on MPRAGE relative to the signal intensity in adjacent muscle (typically the sternocleidomastoid muscle)—referred to in this paper as the relative MPRAGE signal intensity—was calculated in each image at 5-mm intervals extending rostrally along the ICA from the CA bifurcation. Any section of plaque that displayed a signal intensity that was more than 200% that of the adjacent muscle tissue was categorized as having high signal intensity.

Endarterectomy Specimen Processing and Criteria

In symptomatic cases, the mean value of the time from most recent symptoms to CEA was 20.3 ± 28.1 days. The endarterectomy specimens were immediately fixed in Histochoice fixative (Amresco, Inc.) for 48 hours and decalcified with EDTA. Subsequently, they were divided into 5-mm blocks (starting at the CA bifurcation and extending rostrally along the ICA) and embedded in paraffin. From each 5-mm block, a 3-μm section was obtained and stained with H & E and Masson trichrome for histological evaluation. In addition, immunohistochemical testing for glycophorin A was performed to identify IPH (1:200 dilution; Dako). Each section was histopathologically evaluated by an experienced histopathologist (H.I.U.) who was unaware of the MR imaging results. Atheromatous plaques were defined as areas of protrusion into the vascular lumen due to atherosclerosis that were bounded by an internal elastic layer and included fibrous caps. Necrotic core was defined as a core area of atheromatous plaques that consisted of necrotic macrophages, cholesterol crystals, and sometimes hemorrhage. The proportion of the necrotic core area to the total plaque area (NC proportion) was measured using a computer-based morphometric system (WinRoof, Mitani Co.). As an index of the degree of IPH (IPH score), the ratio of the glycophorin A–positive area to the total plaque area was calculated and the sample was graded according to the following scale: a ratio ≥ 0.40 corresponded to a score of 3; a ratio ≥ 0.20 and < 0.40, a score of 2; a ratio < 0.20, a score of 1.

Correlation of MR Imaging and Histological Specimens

The MR images and histological sections were independently reviewed and evaluated. The relative distance from the CA bifurcation was used as a landmark to match the histological data with the MR images in the longitudinal direction of the artery. Morphological features such as lumen size and shape were also used as a reference landmark.

Statistical Analysis

Quantitative variables are presented as the medians and IQRs. The correlation between the relative MPRAGE signal intensity and the NC proportion or IPH score was assessed by nonparametric analysis of the Spearman rank correlation test. The Mann-Whitney U-test was used to compare the NC proportion in samples with high signal intensity on MPRAGE sequences to the proportion in samples with lower signal intensity. Contingency tables displaying IPH scores and MPRAGE signal intensity

(high vs not high) were generated and analyzed by means of the chi-square test to determine a trend. The relationship of IPH score to NC proportion was assessed through nonparametric analysis using the Kruskal-Wallis test. All statistical analyses were performed with StatView (SAS Institute). Differences were considered to be significant when p values were < 0.05.

Results

A total of 96 histological sections corresponding to MR images from 36 endarterectomy specimens were evaluated in this study. Table 1 shows the baseline characteristics of patients, including demographic variables and risk factors.

Correlation Between Size of Necrotic Core and MPRAGE Signal Intensity

Figure 1 shows a scatterplot of the relative MPRAGE signal intensity and the NC proportion. A significant positive correlation was found between the relative MPRAGE signal intensity and the NC proportion ($p = 0.0032$). The NC proportions in plaques with high signal intensity were significantly larger than those in plaques without high signal intensity (median 51.2% [IQR 43.3–66.8%] vs 49.0% [IQR 33.2–57.6%], $p = 0.029$; Fig. 2).

Relationship Between IPH and MPRAGE Signal Intensity

Figure 3 shows a scatterplot of the relative MPRAGE signal intensity and the IPH score. There was a significant positive correlation between the relative MPRAGE signal intensity and the IPH score ($p < 0.0001$). High signal intensity was seen in images corresponding to 14.3, 25.0, and 64.3% of specimens with IPH scores of 1, 2, and 3, respectively. Higher IPH score was significantly associated with high signal intensity on MPRAGE sequences ($p < 0.0001$; Table 2).

Relationship Between IPH and Necrotic Core

The median values (IQRs) for NC proportion were 32.7% (25.3–47.8%), 45.4% (40.5–54.8%), and 53.1% (47.4–65.6%) for samples with IPH scores of 1, 2, and 3, respectively. Higher IPH scores were significantly associated with larger necrotic cores ($p < 0.0001$; Fig. 4).

Representative Examples

Figures 5 and 6 show the representative appearance of MPRAGE images and histological findings from corresponding specimens.

Discussion

Role of IPH in Plaque Progression

Naghavi et al.[19] proposed the concept of vulnerable patients, along with criteria for defining vulnerable plaques, based on autopsy studies of coronary arteries. Among their criteria, IPH has recently been emphasized in pathological studies as an important factor in CA plaque progression.[14,15,32] It has been reported that necrotic core enlargement is crucial for plaque rupture and that increased free cholesterol within the necrotic core is closely associated with lesion instability.[32] Concerning the derivation of free cholesterol, it is generally accepted that apoptotic macrophages are an efficient source of free cholesterol in plaques,[27] although Kolodgie and colleagues[15,32] have demonstrated new lines of evidence suggesting that erythrocyte membranes contribute a significant amount of the free cholesterol in coronary plaques. Nuotio et al.[22] also reported that IPH could play a role in the vulnerability of symptomatic CA plaques by contributing to lipid accumulation and inducing adipophilin (an adipose differentiation-related protein) and further increasing lipid accumulation by preventing lipid efflux. From a symptomatological point of view, Lusby et al.[16] demonstrated that a history of multiple hemorrhage (hemorrhages at various ages) was seen in 81% of patients with symptoms of cerebral ischemia associated with atherosclerotic CA stenosis.

TABLE 1: Summary of demographic and clinical characteristics in 35 patients*

Characteristic	Value
symptomatic lesions	20 (57)
mean degree of stenosis (%)	80 ± 10
mean age in yrs	69 ± 8
female sex	3 (9)
hypertension	24 (69)
diabetes mellitus	15 (43)
hyperlipidemia	19 (54)
cigarette smoking	20 (57)

* Values represent numbers of patients (%) unless otherwise indicated. Means are presented ± SDs.

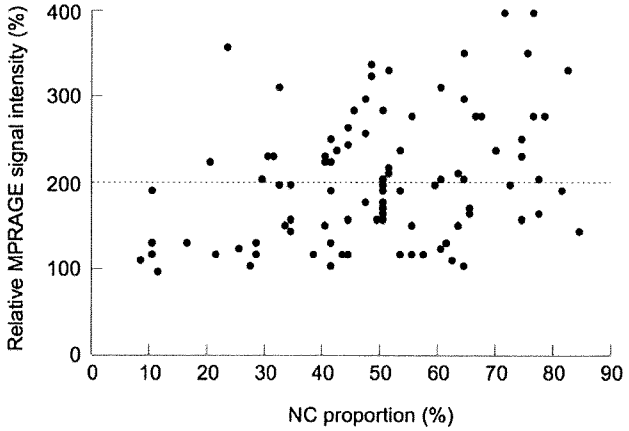

FIG. 1. Scatterplot showing the signal intensity of plaques on MPRAGE sequences relative to the signal intensity in adjacent muscle (relative MPRAGE signal intensity) and the proportion of the necrotic core (NC) area to the total plaque area (NC proportion) as established by pathological examination of specimens. The *broken horizontal line* indicates the level of 200% MPRAGE proportion, the threshold for "high" signal intensity in this study.

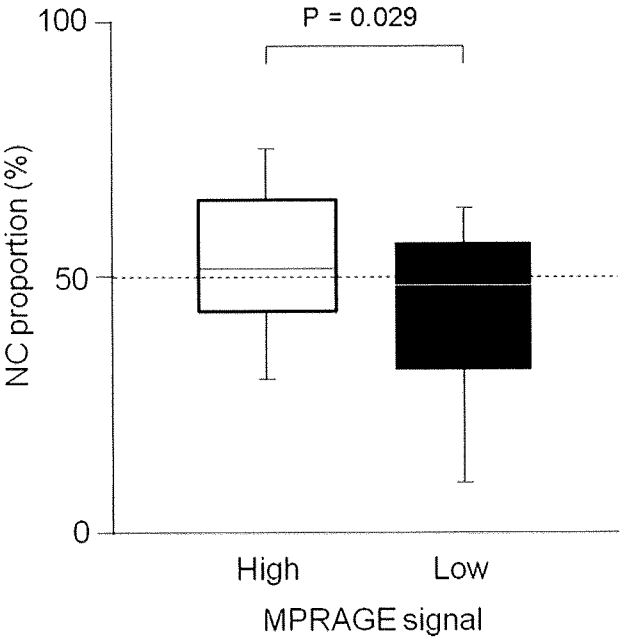

Fig. 2. Box and whisker plot showing the relationship of the NC proportion to MPRAGE signal intensity. The NC proportion in specimens corresponding to imaging studies that showed high signal intensity on MPRAGE sequences was significantly larger than that in specimens that showed lower signal intensity ($p = 0.029$, Mann-Whitney U-test). The *broken horizontal line* is at the level of 50% NC proportion.

The present study demonstrated a significant association of IPH with necrotic core in patients with high-grade CA stenosis. Therefore, the use of a noninvasive and objective modality to detect IPH and to predict subsequent necrotic core expansion in CA plaque could play an important role in assessing plaque vulnerability and in managing patients with CA stenosis in a clinical setting.

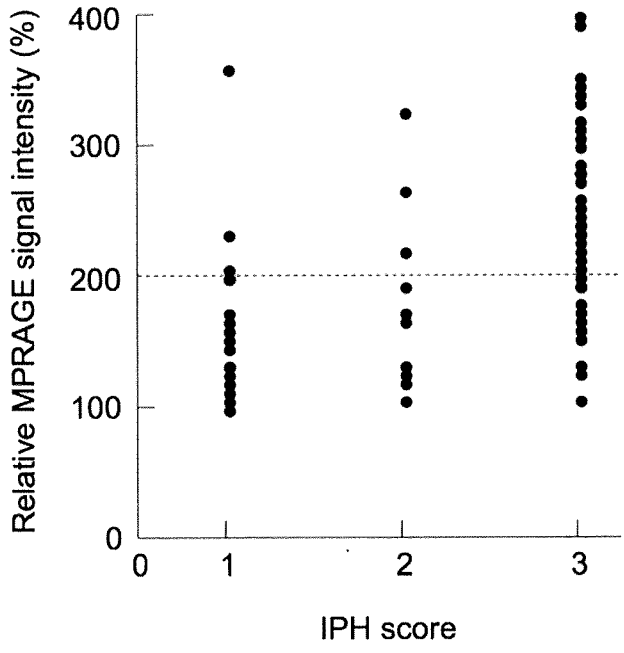

Fig. 3. Scatterplot showing the relative MPRAGE signal intensity and IPH score (1–3). The *broken horizontal line* is at the 200% threshold for high signal intensity.

TABLE 2: Correlation between high signal intensity on MPRAGE sequences in 96 axial MR images and IPH score in corresponding histological sections*

IPH Score	No. of MR Images	Relative Signal Intensity >200%		p Value
		Yes	No	
1	28	4 (14.3)	24 (85.7)	
2	12	3 (25.0)	9 (75.0)	<0.0001
3	56	36 (64.3)	20 (35.7)	

* Signal intensity in CA plaque was assessed relative to that of adjacent muscle tissue, using 200% as the threshold for "high" signal intensity on MPRAGE sequences. Values represent numbers of images, expressed as a percentage of the images in the given score category in parentheses.

Assessment of Carotid Plaque by MPRAGE Sequence

Moody et al.[17] used a T1-weighted magnetization-prepared 3D gradient echo sequence, a technique identical to that used in MPRAGE, to detect complicated plaque by detecting IPH in an in vivo study of CA plaques in symptomatic patients. Bitar et al.[4] recently reported that MR imaging of IPH using a 3D spoiled gradient-echo sequence resulted in strong agreement between imaging and histologic findings. Yamada et al.[33] disclosed significant associations between cerebral ischemic events and MPRAGE hyperintensity according to stenosis severity using 200% of the signal intensity of adjacent muscle as the threshold for high signal intensity and reported the percentages of patients with high signal intensity were 21, 54, and 65% for mild (0–29%), moderate (30–69%), and severe (70–99%) stenosis, respectively. The present study demonstrated that the NC proportion in plaques with high signal intensity on MPRAGE sequences was significantly larger than that in plaques with lower signal intensity, and the severity of IPH was significantly correlated with signal intensity. The hemorrhage-rich larger necrotic core is a pathological basis for the high signal intensity on MPRAGE in these plaques, which has previously been shown to be significantly associated with symptomatology.[33] Also, in the present study, 58% of CAs examined (21 of 36) had high signal intensity on MPRAGE sequences and 58% of the endarterectomy sections (56 of 96) exhibited the highest degree of IPH (score of 3 in our pathological examination). Together with the data from Yamada et al.,[33] the data from this study shows, through the association between MPRAGE signal hyperintensity and high-grade CA stenosis, that IPH has a high prevalence in advanced CA atherosclerotic plaques; our data also raise the possibility that IPH is a major mechanism underlying the progression of stenosis through its stages of severity as well as the expansion of the necrotic core.

The majority of previous reports have used multiple contrast techniques (T1-weighted, T2-weighted, proton-density–weighted, and 3D time-of-flight MR imaging)

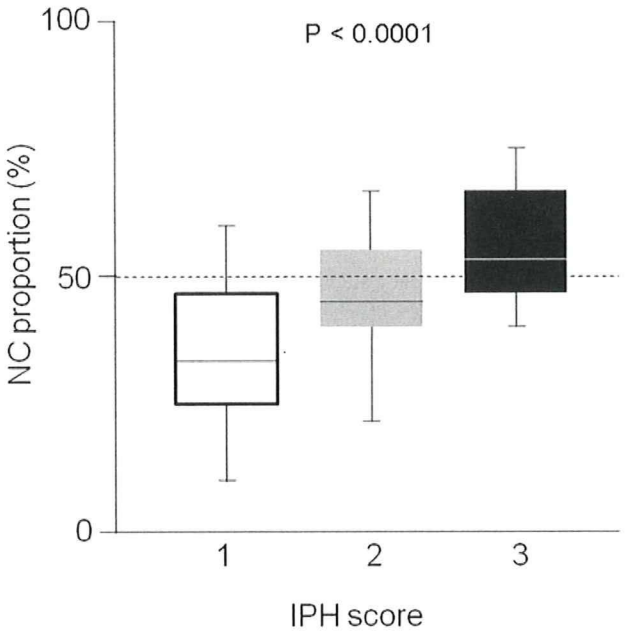

Fig. 4. Box and whisker plot showing the relation of IPH score to NC proportion. Higher IPH scores were significantly associated with higher NC proportion, according to the Kruskal-Wallis test ($p < 0.0001$). The *broken horizontal line* is at the level of 50% NC proportion.

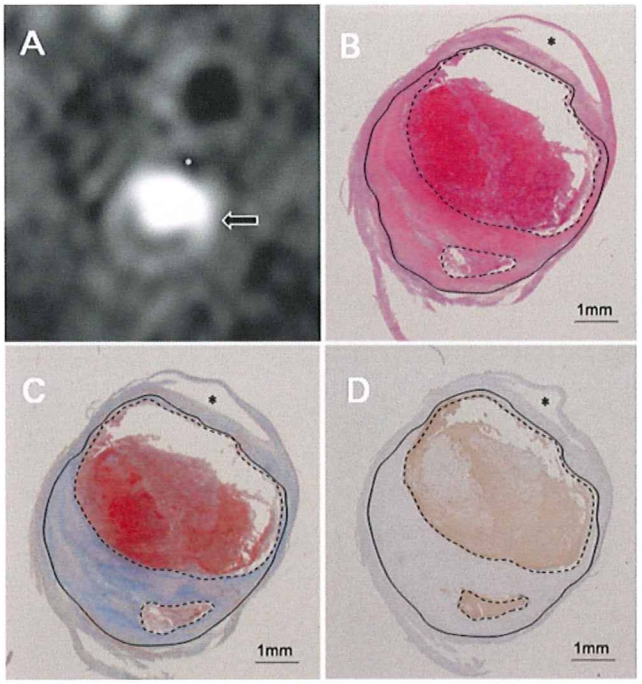

Fig. 5. An example of plaque with high signal intensity. **A:** An MPRAGE image showing the plaque *(arrow)*. **B and C:** Photomicrographs of histological sections showing a large amount of necrotic core with IPH. H & E **(B)** and Masson trichrome **(C)**. **D:** Photomicrograph showing that the necrotic core is strongly positive for glycophorin A. *Asterisks* indicate the ICA lumen. The total plaque area is delineated by a *solid line* and the necrotic core area by a *dotted line*. Bar = 1 mm.

to identify necrotic cores and IPH.[6,13,28,29,34] Saam et al.[25] demonstrated the accuracy and reproducibility of using multicontrast imaging to quantify CA plaque components. On the other hand, the usefulness of single-contrast imaging using a 3D gradient-echo sequence has also been demonstrated.[1,4,17,18,33] This sequence is often employed to identify IPH using a T1-weighted signal alone. In a study comparing the performance of a gradient-echo sequence with that of a spin-echo sequence, the gradient-echo sequence had a higher detection rate for IPH as well as much better interobserver agreement and better image quality.[5] Likewise, Ota et al.[23] reported that the MPRAGE sequence at 3 T had the highest diagnostic capability for the detection and quantification of IPH, in a study comparing it with the fast spin echo and spoiled gradient echo sequences. In the present study, the area over which MPRAGE signal hyperintensity was present in CA plaque was not directly compared with the area of the necrotic core as measured through histopathological analysis. Nevertheless, our data reveal that the areas of high signal intensity on MPRAGE sequences coincide with the hemorrhage-rich large necrotic core. As the interpretation of MPRAGE signal intensity is simple and objective, requiring only a short image acquisition time (5 minutes), this 3D gradient-echo sequence technique is useful in a clinical setting.

As the practice of CA stent placement has rapidly become more prevalent, distal embolic complications during the procedure have become an important clinical issue. A report on the use of a filter protection device during CA stent placement in Japan revealed that disturbed blood flow presumably due to the blockage of the filter pores by plaque was observed in 40.0% of cases (slow flow in 26.7%, no flow in 13.3%).[30] Angeneli et al.[2] collected the embolized debris caught in such a filter and performed histopathological analysis on it; they reported that the collected debris consisted predominantly of thrombotic material, foam cells, and cholesterol clefts. The use of MPRAGE for CA plaque analysis before CA stent placement could be useful in predicting the risk of embolic complication and blood flow disturbances and could aid in selecting suitable distal protection devices.

Study Limitations

First, we used immunohistochemical staining for glycophorin A as a marker of IPH. Glycophorin A is a protein specific to erythrocytes that facilitates anion exchange; it is also an indicator of previous hemorrhage.[15] Although high signal intensity on MPRAGE sequences was associated with the detection of previous hemorrhages by glycophorin A, the signal hyperintensity may not be related to fresh thrombi or hemorrhages. In fact, in this study, a few endarterectomy sections with fresh thrombi revealed only lower-intensity signals. Because fresh thrombi play a crucial role in the pathogenesis of stroke,[26] it is important to detect them and to accurately classify IPH; thus, if MPRAGE is to become a useful technique, we must develop sequences that can detect fresh thrombi and also measure the age of IPH lesions. Second, because the patients included in this study had been selected as candidates for CEA based on the criteria of our institute,[12]

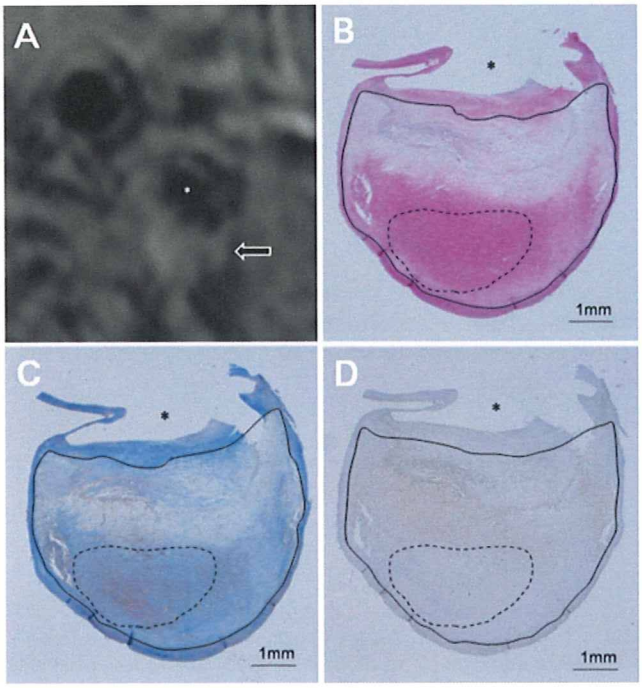

Fig. 6. An example of plaque with lower signal intensity. **A:** An MPRAGE image showing the plaque *(arrow)*. **B and C:** Photomicrographs of ICA sections show the plaque is mainly consisted of fibrous tissue and focal calcification. H & E **(B)** and Masson trichrome **(C)**. **D:** Photomicrograph showing that the plaque is only lightly stained for glycophorin A. *Asterisks* indicate the ICA lumen. The total plaque area is delineated by a *solid line* and the necrotic area by a *dotted line*. Bar = 1 mm.

pathological examination and MR imaging analysis in this study were restricted to patients with high-grade stenosis. Yet the relative risk of ipsilateral ischemia according to MPRAGE signal intensity was reported to be the highest in the moderate-stenosis group.[33] In future studies of MPRAGE, it would be better to investigate the pathological differences between patients with moderate stenosis and high signal intensity and those with moderate stenosis and lower signal intensity.

Conclusions

We demonstrated that in CA plaque with high-grade stenosis, high signal intensity on MPRAGE sequences (> 200% increase relative to signal intensity in adjacent muscle tissue) indicates larger necrotic cores and more severe degrees of IPH than lower signal intensity. We also found that IPH is closely associated with necrotic core expansion in advanced CA plaque. These results indicate that MPRAGE, a T1-weighted imaging technique, can accurately reveal plaque progression in conjunction with IPH in patients with high-grade stenosis.

Disclosure

The authors report no conflict of interest concerning the materials or methods used in this study or the findings specified in this paper.

Author contributions to the study and manuscript preparation include the following. Conception and design: T Hishikawa, K Iihara. Acquisition of data: N Yamada, H Ishibashi-Ueda. Reviewed final version of the manuscript and approved it for submission: T Hishikawa, K Iihara, N Yamada, H Ishibashi-Ueda, S Miyamoto. Study supervision: S Miyamoto.

References

1. Altaf N, MacSweeney ST, Gladman J, Auer DP: Carotid intraplaque hemorrhage predicts recurrent symptoms in patients with high-grade carotid stenosis. **Stroke 38:**1633–1635, 2007
2. Angelini A, Reimers B, Della Barbera M, Saccà S, Pasquetto G, Cernetti C, et al: Cerebral protection during carotid artery stenting: collection and histopathologic analysis of embolized debris. **Stroke 33:**456–461, 2002
3. Barnett HJ, Taylor DW, Eliasziw M, Fox AJ, Ferguson GG, Haynes RB, et al: Benefit of carotid endarterectomy in patients with symptomatic moderate or severe stenosis. The North American Symptomatic Carotid Endarterectomy Trial Collaborators. **N Engl J Med 339:**1415–1425, 1998
4. Bitar R, Moody AR, Leung G, Symons S, Crisp S, Butany J, et al: In vivo 3D high-spatial-resolution MR imaging of intraplaque hemorrhage. **Radiology 249:**259–267, 2008
5. Cappendijk VC, Cleutjens KBJM, Heeneman S, Schurink GWH, Welten RJTJ, Kessels AGH, et al: In vivo detection of hemorrhage in human atherosclerotic plaques with magnetic resonance imaging. **J Magn Reson Imaging 20:**105–110, 2004
6. Chu B, Kampschulte A, Ferguson MS, Kerwin WS, Yarnykh VL, O'Brien KD, et al: Hemorrhage in the atherosclerotic carotid plaque: a high-resolution MRI study. **Stroke 35:**1079–1084, 2004
7. European Carotid Surgery Trialists' Collaborative Group: MRC European Carotid Surgery Trial: interim results for symptomatic patients with severe (70-99%) or with mild (0-29%) carotid stenosis. European Carotid Surgery Trialists' Collaborative Group. **Lancet 337:**1235–1243, 1991
8. Executive Committee for the Asymptomatic Carotid Atherosclerosis Study: Endarterectomy for asymptomatic carotid artery stenosis. **JAMA 273:**1421–1428, 1995
9. Fox AJ: How to measure carotid stenosis. **Radiology 186:**316–318, 1993
10. Golledge J, Greenhalgh RM, Davies AH: The symptomatic carotid plaque. **Stroke 31:**774–781, 2000
11. Halliday A, Mansfield A, Marro J, Peto C, Peto R, Potter J, et al: Prevention of disabling and fatal strokes by successful carotid endarterectomy in patients without recent neurological symptoms: randomised controlled trial. **Lancet 363:**1491–1502, 2004
12. Iihara K, Murao K, Sakai N, Yamada N, Nagata I, Miyamoto S: Outcome of carotid endarterectomy and stent insertion based on grading of carotid endarterectomy risk: a 7-year prospective study. **J Neurosurg 105:**546–554, 2006
13. Kampschulte A, Ferguson MS, Kerwin WS, Polissar NL, Chu B, Saam T, et al: Differentiation of intraplaque versus juxtaluminal hemorrhage/thrombus in advanced human carotid atherosclerotic lesions by in vivo magnetic resonance imaging. **Circulation 110:**3239–3244, 2004
14. Kolodgie FD, Burke AP, Nakazawa G, Cheng Q, Xu X, Virmani R: Free cholesterol in atherosclerotic plaques: where does it come from? **Curr Opin Lipidol 18:**500–507, 2007
15. Kolodgie FD, Gold HK, Burke AP, Fowler DR, Kruth HS, Weber DK, et al: Intraplaque hemorrhage and progression of coronary atheroma. **N Engl J Med 349:**2316–2325, 2003
16. Lusby RJ, Ferrell LD, Ehrenfeld WK, Stoney RJ, Wylie EJ: Carotid plaque hemorrhage. Its role in production of cerebral ischemia. **Arch Surg 117:**1479–1488, 1982

17. Moody AR, Murphy RE, Morgan PS, Martel AL, Delay GS, Allder S, et al: Characterization of complicated carotid plaque with magnetic resonance direct thrombus imaging in patients with cerebral ischemia. **Circulation 107:**3047–3052, 2003
18. Murphy RE, Moody AR, Morgan PS, Martel AL, Delay GS, Allder S, et al: Prevalence of complicated carotid atheroma as detected by magnetic resonance direct thrombus imaging in patients with suspected carotid artery stenosis and previous acute cerebral ischemia. **Circulation 107:**3053–3058, 2003
19. Naghavi M, Libby P, Falk E, Casscells SW, Litovsky S, Rumberger J, et al: From vulnerable plaque to vulnerable patient: a call for new definitions and risk assessment strategies: Part I. **Circulation 108:**1664–1672, 2003
20. Nighoghossian N, Derex L, Douek P: The vulnerable carotid artery plaque: current imaging methods and new perspectives. **Stroke 36:**2764–2772, 2005
21. North American Symptomatic Carotid Endarterectomy Trial Collaborators: Beneficial effect of carotid endarterectomy in symptomatic patients with high-grade carotid stenosis. **N Engl J Med 325:**445–453, 1991
22. Nuotio K, Isoviita PM, Saksi J, Ijäs P, Pitkäniemi J, Sonninen R, et al: Adipophilin expression is increased in symptomatic carotid atherosclerosis: correlation with red blood cells and cholesterol crystals. **Stroke 38:**1791–1798, 2007
23. Ota H, Yarnykh VL, Ferguson MS, Underhill HR, DeMarco JK, Oikawa M, et al: Comparison between three T1-weighted sequences for detection and area measurement of intraplaque hemorrhage in carotid atherosclerotic plaque imaging at 3 tesla. **Proc Intl Soc Mag Reson Med 17:**605, 2009 (Abstract)
24. Rothwell PM, Gutnikov SA, Warlow CP: Reanalysis of the final results of the European Carotid Surgery Trial. **Stroke 34:**514–523, 2003
25. Saam T, Ferguson MS, Yarnykh VL, Takaya N, Xu D, Polissar NL, et al: Quantitative evaluation of carotid plaque composition by in vivo MRI. **Arterioscler Thromb Vasc Biol 25:**234–239, 2005
26. Spagnoli LG, Mauriello A, Sangiorgi G, Fratoni S, Bonanno E, Schwartz RS, et al: Extracranial thrombotically active carotid plaque as a risk factor for ischemic stroke. **JAMA 292:**1845–1852, 2004
27. Tabas I: Consequences of cellular cholesterol accumulation: basic concepts and physiological implications. **J Clin Invest 110:**905–911, 2002
28. Takaya N, Yuan C, Chu B, Saam T, Polissar NL, Jarvik GP, et al: Presence of intraplaque hemorrhage stimulates progression of carotid atherosclerotic plaques: a high-resolution magnetic resonance imaging study. **Circulation 111:**2768–2775, 2005
29. Takaya N, Yuan C, Chu B, Saam T, Underhill H, Cai J, et al: Association between carotid plaque characteristics and subsequent ischemic cerebrovascular events: a prospective assessment with MRI—initial results. **Stroke 37:**818–823, 2006
30. Takayama K, Nakagawa H, Iwasaki S, Taoka T, Miyasaka T, Myouchin K, et al: Initial experience of using the filter protection device during carotid artery stenting in Japan. **Radiat Med 26:**348–354, 2008
31. Virmani R, Burke AP, Kolodgie FD, Farb A: Pathology of the thin-cap fibroatheroma: a type of vulnerable plaque. **J Interv Cardiol 16:**267–272, 2003
32. Virmani R, Kolodgie FD, Burke AP, Finn AV, Gold HK, Tulenko TN, et al: Atherosclerotic plaque progression and vulnerability to rupture: angiogenesis as a source of intraplaque hemorrhage. **Arterioscler Thromb Vasc Biol 25:**2054–2061, 2005
33. Yamada N, Higashi M, Otsubo R, Sakuma T, Oyama N, Tanaka R, et al: Association between signal hyperintensity on T1-weighted MR imaging of carotid plaques and ipsilateral ischemic events. **AJNR Am J Neuroradiol 28:**287–292, 2007
34. Yuan C, Mitsumori LM, Ferguson MS, Polissar NL, Echelard D, Ortiz G, et al: In vivo accuracy of multispectral magnetic resonance imaging for identifying lipid-rich necrotic cores and intraplaque hemorrhage in advanced human carotid plaques. **Circulation 104:**2051–2056, 2001

Manuscript submitted July 13 2009.
Accepted March 1, 2010.
Please include this information when citing this paper: published online April 9, 2010; DOI: 10.3171/2010.3.JNS091057.
Address correspondence to: Tomohito Hishikawa, M.D., Department of Neurological Surgery, Okayama University Graduate School of Medicine and Dentistry, 2-5-1 Shikata-cho, Okayama City, Okayama, 700-8558 Japan. email: t-hishi@md.okayama-u.ac.jp.